NASA Contractor Report 4130

Tabulation of Mie Scattering Calculation Results for Microwave Radiative Transfer Modeling

Hwa-Young M. Yeh and N. Prasad

CONTRACTS NAS5-30143 and NAS5-28795
MARCH 1988

NASA

NASA Contractor Report 4130

Tabulation of Mie Scattering Calculation Results for Microwave Radiative Transfer Modeling

Hwa-Young M. Yeh
Caelum Research Corporation
Silver Spring, Maryland

N. Prasad
General Sciences Corporation
Laurel, Maryland

Prepared for
Goddard Space Flight Center
under Contracts NAS5-30143 and NAS5-28795

National Aeronautics
and Space Administration

**Scientific and Technical
Information Division**

1988

ACKNOWLEDGEMENTS

The authors would like to thank Drs. Robert Adler and Joanne Simpson for their continuous encouragement and support on this work, and Drs. Alfred Chang, Chris Kummerow and Warren Wiscombe for the helpful discussions and comments. This work has been performed under NASA Contract NAS5-30143 and NAS5-28795. The support of this program by Dr. James Dodge at NASA Headquarters is greatly appreciated.

PREFACE

In microwave radiative transfer model simulations, the Mie calculations usually consume the majority of the computer time necessary for the calculations (70 to 86 % for frequencies ranging from 6.6 to 183 GHz). For a large array of atmospheric profiles, the repeated calculations of the Mie codes make the radiative transfer computations not only expensive, sometimes impossible. It is desirable, therefore, to develop a set of Mie tables to replace the Mie codes for the designated ranges of temperature and frequency in the microwave radiative transfer calculation.

In this study, we have only developed the Mie tables for the microwave region, because (a) it is our interest to understand the microwave radiative transfer processes in cloudy and precipitating atmospheres, and (b) it is more feasible to construct a Mie table in the microwave frequencies than other spectral regions. The tables are divided into two major categories of ice and liquid water, because the two phases have distinctive scattering and absorption characteristics. The Mie tables for liquid water are further divided into two parts to save computer storage space; one for low frequencies (below 37 GHz) and the other for high frequencies (up to 300 GHz).

Results of using the Mie tables in the microwave radiative transfer calculations show the total CPU time (IBM 3081) used for the modeling simulation is reduced by a factor of 7 to 16, depending on the frequency. The tables are tested by computing the upwelling radiance of 144 atmospheric profiles generated by a three-dimensional cloud model (Tao, 1986). Results are compared with those using Mie quantities computed from the Mie codes. The bias and root-mean-square deviation (RMSD) of the model results using the Mie tables, in general, are less than 1 K except for 37 and 90 GHz. Over all, neither the bias nor RMSD is worse than 1.7 K for any frequency and any viewing angle.

TABLE OF CONTENTS

LIST OF TABLES

LIST OF FIGURES

1. INTRODUCTION

Remote sensing techniques for atmospheric study, especially estimation of precipitation amount and intensity have been developed over the last two decades using satellite data at visible, infrared, and microwave frequencies. Many of these methods are empirical relationship between cloud signatures in satellite imagery and ground truth from radar or rainfall networks. Among those frequency regions, the microwave techniques offer a more physically based method, because the microwave upwelling radiation is more physically related to precipitation in the atmosphere. Development of microwave radiative transfer models for precipitation or cloudy atmospheres is of fundamental importance for retrieval and inference of cloud liquid water content and rainfall rate. The microwave radiative transfer modeling serves three basic purposes: (1) to better understand the relationship of microwave radiances to atmopheric properties including cloud structure and rainfall distribution; (2) to better interpret aircraft and spaceborne microwave radiometer data; and (3) to develop remote sensing techniques based on model simulation and measurement experiments. In the past, study of the transfer of microwave radiation in cloudy and/or precipitating atmospheres has been limited to utilizing a Rayleigh scattering approximation (*e.g.* Weinman and Guetter, 1977), because it was believed that the scattering from solid or liquid water droplets in the atmosphere had minimal effect on the microwave upwelling radiances. Although the Mie theory has been used for calculation of scattering from rainwaters (e.g. Yeh and Liou, 1983), it was not until recent years that scattering from ice particles in the atmosphere has been shown an important effect on measured microwave radiances (*e.g.* Wilheit *et al.*, 1982; Yeh *et al.*, 1983; Wu and Weinman, 1984; Szejwach *et al.*, 1986).

For radiative transfer modeling simulation, Mie theory has been conventionally utilized to calculate the scattering and extinction parameters. Although Mie theory can only be applied to the scattering by spheres, it represents the most complete calculation available for the particle scattering problem. It is apparent that few particles are spherical in nature; falling rain drops are elongated, many hailstones have nonconcentric cores, and snowflakes are well known for their intricate forms. The scattering effect of nonspherical particles that are much smaller than the wave-

length is governed by their polarizability tensor (*e.g.* van de Hulst, 1957). Particle of simple shape that are much larger than the wavelength may be treated by a combination of geometrical optics and Fraunhofer diffraction (*e.g.* Jacobowitz, 1971; Liou, *et al.*, 1983). At intermediate sizes, fancy theoretical methods for relatively simple shapes are needed to solve the problems frequently encountered. Recent advances in electromagnetic scattering theory now make it possible to calculate exact scattering phase matrix elements for certain nonspherical dielectric objects of intermediate sizes. Asano and Sato (1980), for example, reported comprehensive single scattering and polarization results for randomly oriented, identical spheroidal particles utilizing the solution of the wave equation in spheroidal coordinates. Although their solution is exact, their computations are complicated and lengthy, particularly for larger particles and for averages over all orientations, not to mention size and shape distributions. Because of this, perhaps, the spheroidal solution has been slow to be adapted by other workers. Because the majority of scattering particles are not spherical, the Mie theory does not strictly apply to them. The experimental evidence, however, indicates that with averaging over orientation and size, mildly nonspherical particles scatter very much like equivalent spheres (*e.g.* Zerull, 1976). This certainly enhances the utility of the Mie solution, and a wide range of applications of Mie calculation are then possible.

Mie scattering calculations have been developed and improved for efficiency in the past (*e.g.* Wiscombe, 1980), but are still known for being time-consuming. One of the major reasons is that in typical applications, one has to repeat the Mie scattering calculation for a large number of radii over particle size distributions, a large number of wavelengths across a spectrum, and a wide range of temperatures. For a radiative transfer calculation at five different wavelengths, if we divide the atmosphere into 20 regions for cloud and precipiation, and up to four classes of particle (cloud water cloud and ice, rainwater and graupel) may coexist in each region, we may need to repeat the Mie scattering calculation at least ten thousand times. The problem becomes much worse if a large array of radiative transfer calculation is needed for the simulation of upwelling brightness temperatures over a region. For instance, if one applies the results of a three-dimensional cloud model in a radiative transfer model to obtain the brightness temperatures over a region gridded by a 10×10 horizontal spatial array (given any spatial resolution), more than a million scattering calculations are required for the complete simulation. Table 1 shows that for an atmospheric profile used by Wu and Weinman (1984; shown in Fig.

1) for rain rate (RR) at 64 mm/hr, the Mie calculation approximately consumes 80% of total CPU (Central Processing Unit) time for 37 GHz in the iterative radiative transfer model used in the Goddard Laboratory for Atmospheres. The percentage of CPU consumption is dependent on the frequency as shown in the table. It would be much more efficient for modeling simulations if one pre-calculated the Mie scattering for the designated ranges of particle radii, wavelengths and temperatures and tabulated the results for the use in radiative transfer calculations.

In the past, as Van de Hulst (1957) notes there have been some ambitious tabulations of various Mie quantities, they are useful mostly only for checking computer codes. Wiscombe (1979) cautioned that because of the rapid oscillation of most Mie quantities, these variations would be impossible to resolve in a comprehensive table. While recognizing there are resonances (sharp spikes) within Mie quantities whose scale is much finer even than the oscillations, we intend to make a Mie table limited to ranges of microwave frequencies and realistic hydrometeor's size spectrum, and under normal atmospheric conditions. We take advantage of the fact that most of the effective hydrometeors' sizes are relatively small in comparison with the microwave wavelength; a range of size parameter (x) up to 20 would be sufficient for the table. Here, the x is defined as a ratio of the particle circumference ($2\pi r$, r is particle's radius) to wavelength of the incident radiation.

The Mie tables include three input variables of size parameter, real and imaginary refractive indices and output of Mie calculations including scattering and extinction efficiency factors and four phase functions. The phase function is tabulated as a function of scattering angles θ. No more than 90 phase angles are needed to accurately reproduce each phase function, and for some tables, 20 phase angles are sufficiently accurate. The entire Mie table is divided into two major categories of liquid water and ice, because the two phases have distinctive scattering and absorption characteristics. The total number of records for the ice table is 2681 and each record consists of one set of input and output of the Mie quantities Each set of Mie quantities has a total of 365 real numbers including three input variables, extinction and scattering efficiency factors, and phase functions, which consist of four element and each element is represented by 90 averaged angles in the ice table. The Mie tables for liquid water are further devided into two parts for efficiency; one is for low frequencies (below 37 GHz) and the other is for high frequencies (up to 300 GHz). The total number of records for the high frequencies is 2414 with

each record having 365 real numbers; and for the low frequencies, the total record number is 4700 with 85 real numbers for each record. For the high frequency part, each element of phase functions is represented by 90 averaged angles, but for the low frequency part, 20 averaged angles are found sufficient for the water tables.

2. BACKGROUND

Mie scattering is dependent on two factors: complex refractive index (m) and size parameter (x). The parameter m is a function of temperature and wavelength; and x is a function of the particle's radius and wavelength of the incident radiation. The Mie calculation results are tabulated by using m and x as input variables instead of electromagnetic wavelength of the incident radiation (L), temperature (T) and particle size (r). Fig. 2 shows that m as a function of T and L, and x as a function of L and r; the Mie scattering calculation results are tabulated starting from below the dashed-line. The Mie calculation results include three parameters: extinction efficiency factor (Q_e), scattering efficiency factor (Q_s), and phase function $P(\theta)$. The phase function is tabulated as a function of scattering angles θ. The phase functions include four elements giving the quantities of the total intensity, the degree of polarization, the plane of polarization, and the ellipticity of the electromagnetic wave at each point and in any given direction. Usually, the first two elements of the phase functions are more interesting, and have a greater effect on the radiative transfer calculation. The m and x need to be computed in the radiative transfer model before the Mie table can be applied. Those computations are usually quite simple and consume little computer time.

The most crucial procedure in constructing the Mie table is to determine the range and resolution for the input variables, m and x, to be used in the Mie calculations. On one hand, we would like to have the tables cover as wide a range of m and x as possible, and tabulate the Mie results in as much detail as possible. On the other hand, we need to have an efficient Mie table for practical applications. In principle, we can not trade off the accuracy for the efficiency in compilation of the tables; however, in some circumstances, a finer resolution of the table does not always improve the accuracy of the Mie results, but only wastes computer storage space. The resolution of the tables should not be set uniformly, it should rather depend on the behavior of Mie scattering properties in different regions of m and x. For instance, a finer resolution of x is necessary when x is small, but the resolution should be increased when x becomes large. The coarser resolution of x not only makes the table more efficient, but also averages out the unwanted ripples of the Mie results.

2.1 Complex Refractive Index

The complex refractive index is an optical parameter associated with the velocity change of an electromagnetic wave in a medium with respect to vacuum. The complex refractive index consists of real part (n) and imaginary part (k);

$$m(\nu) = n(\nu) - ik(\nu) \tag{1}$$

ν is the frequency of the electromagnetic wave in vacuum, and $\nu = c/L$, where c is the speed of light (3×10^{10} cm/sec). Both the real and imaginary indices are related to the scattering and absorption properties of particles; n relates to the phase velocity of propagation in the material and k is the absorption index, which is related to the absorption coefficient κ_{abs}, as

$$\kappa_{abs} = 4\pi k/L \tag{2}$$

In the microwave and radiowave spectra, it is quite usual to report the complex relative permittivity ε in the laboratory measurements. While the complex refractive index is used in the Mie calculation, one may relate the ε to the complex refractive index by $m^2 = \varepsilon$. The optical constants of ice and liquid water have been reviewed, respectively, by Warren (1984) and Ray (1972) for the entire spectrum including infrared, microwave, and radiowave regions. For liquid water, the determination of m is rather well known, except for supercooled water and at the frequencies between 50 and 300 GHz. The uncertainty of m is mostly due to lack of experimental data to confirm the formulae used to derive the values of m. For ice, no reliable measurements of absorption properties are available, especially for temperatures T between 0° and −60°C at microwave wavelengths between 1 and 30 mm (frequency 300 and 10 GHz) (*e.g.* Warren, 1984; Evans, 1965). Interpolation and extrapolation from the existing data at other temperatures and frequencies are necessary to obtain the values of m for the desired range of temperature in the microwave region.

In the Mie table, the n and k are treated as two independent variables except for ice phase which has an approximately constant value of n in the microwave region. Since the formulae used for computing m, so far, are not conclusive for both ice and liquid water, the advantage of using m and x as input for the tables is obvious; if L, T, and r are input variables for the table, the formulae for computing m from T and L will have to be fixed and the tables will lose their flexibility. In

our procedure, if other formulae are found to be more suitable for computing m, the Mie tables will not need to be recompiled to fit the new formula.

Figs. 3 and 4 show the complex refractive indices for liquid water as computed from empirical formulae of Ray (1972) and Lane and Saxton (1952), respectively. The figures demonstrate the differences of the results from the two formulae, especially the treatment of supercooled water in the high frequency (or short wavelength) region. In both figures, we mark the frequencies of 5, 37, and 183 GHz at different temperatures. Poorer agreement appears to occur in higher frequencies and sub-freezing regions, although the work of Lane and Saxton is the only source of providing sub-freezing (as cold as $-8°$C) data of m in the empirical formula of Ray. The formulae given by Ray were essentially extensions of Debye theory by Cole and Cole (1941). The ranges of m given in our Mie tables, as shown the non-shaded area in the figures, are mostly based on the formula by Ray.

Although this Mie table will not be restricted to certain formulae for computing m, the extended Debye theory is used in providing us a sense of the range of m values for the designated regions of temperature and wavelength. For liquid water, the temperature ranges from 40°C to $-40°$C and the frequency from 5 to 300 GHz. The ranges of m values to be tabulated in the tables are restricted to the corresponding temperature and frequency ranges. The values of m in the shaded areas of Figs. 3 and 4 do not occur in realistic atmospheres for the microwave region, and will not be included in the tables. The extended Debye theory, as discussed in Ray (1972), fits the experimental data very well for the frequencies below 50 GHz ($L > 6$ mm) and above 300 GHz ($L < 1$ mm). Between 50 and 300 GHz, few measured data are available; however, the smooth transition of m values in this region is assumed based on the extended Debye theory.

For ice, the real index of refraction is obtained by reflectance measurements from a plane-shave ice block. The Fresnel formulae give real refractive index n unambiguously if imaginary refractive index k is small. The n is thus known reliably, and independently of k, in the regions of weak absorption. At all wavelengths short of the dielectric relaxation, the real index of ice is of the order unity, but the imaginary index, by contrast, varies over the range from 10^{-9} to 1. In the microwave region, the real index is known as an approximately constant value of 1.78 for the entire spectrum, and the imaginary index is in the order from 10^{-4} to 10^{-2}. For liquid water, the refractive index has a large imaginary component ($k >> 0.01n$)

in the microwave region, the Fresnel reflectivity is no longer dominated by n but also contains a measureable contribution due to k. The dielectric properties of ice and water are therefore dramatically different over $\sim$7 orders of magnitude in the microwave region; water is highly reflective and absorptive, but ice is quite transparent.

There is no strong absorption band in the microwave region for ice, and the conductivity is independent of frequency as measured by Worz and Cole (1969). They measured the dielectric parameters for the Debye equations. Their approach was adjusted to include the spread parameter and static constant so that $n = 1.78$ over the entire microwave spectrum and k agreed with the values found by Cumming (1957) at 3.2 cm as a function of temperature (Ray, 1972). Although there are no reliable measurements of k between 1 and 30 mm, one can be sure that there is no strong absorption band in the unmeasured region, because the infrared absorption bands fully account for the measured microwave n (Warren, 1984). This is also substantiated by the qualitative observation of Champion and Sievers (1980) that ice is "completely transparent" at wavelength of 2.5 mm. In the process of constructing the Mie tables, we discovered that the results of the microwave radiative transfer calculations are not sensitive to the variation of k as long as the value of k remains small ($\sim$ 3 orders of magnitude smaller than n).

2.2 Size Parameter

The other input variable in the Mie table is the size parameter (x), which is defined by $2\pi r/L$. The major maxima and minima of the scattering and extinction efficiency factors (Q_s and Q_e, respectively) for $1 < x < 10$ are due to the interference of radiation diffracted and transmitted by the sphere; whereas the ripples arise from edge rays that are grazing and traveling the sphere, spewing off energy in all directions. Q_s and Q_e increase rapidly as x reaches about 2.5 and approach an asymptotic value when x continues to increase. For ice, as shown in Figs. 5a and b, the curves of Q_s and Q_e are very close to each other, because the absorption of microwave radiation is very small for ice particles. For liquid water, both the ripples and the major maxima and minima damp out as absorption within the particle increases (Fig. 6a and b). The peaks of the scattering efficiency factor between $x = 2$ and 4 severely affect the radiative transfer calculation whenever the particle size distribution with significant concentration extends over this area. Since

the Mie scattering quantities tend to approach an asymptotic value after $x = 20$ (Fig. 5), we may use an averaged value of Mie quantities between $x = 20$ and 22 to represent the values of x beyond 20. One should be aware that only exceptionally large size of hydrometeors can cause x to exceed 20 in the microwave region (*e.g.* $r > 6.5$ mm at 183 GHz).

In Figs. 5a and b, for 180 and 18 GHz, respectively, the size distributions of the ice cloud, obtained from the aircraft measurements during the Cooperative Convective Precipitation Experiment (CCOPE) as discribed by Heymsfield (1986), are plotted over the x scale for Mie scattering of ice particles at $-30°$C. The aircraft measurements, collected ice particles in mid- to lower levels at temperatures from $-25°$C to $-36°$C, show that the size spectra broaden with decreasing altitude. The ice particle size distribution as shown in Figs. 5a and b are based on the measurements at the lower altitude of 8.0 km. For liquid water, both the ripples and the major maxima and minima damp out as absorption within the particle increases. In the study of functional fits to observed drop size distributions, Willis (1984) applys five different functional fits to the drop size distribution at different rainfall rate based on the data sample of airborne optical spectrometer measurements obtained in two tropical cyclones. Figs. 6a and b show the drop size distribution of the precipitation using the Marshall-Palmer exponential fits for the rain rate at 169 mm/hr. The drop size distribution is plotted on both 180 and 18 GHz, respectively, for the Mie scattering of liquid water droplets at $T = 20°$C. They explain that for the same size distributions, the scattering effects from particles for 180 and 18 GHz are very different; the same particle size spectrum essentially covers different portions of x for different frequencies. Since the characteristics of the Mie quantities are quite different at different x, the resolution and range of x in the table thus need to be considered separately for various frequencies. This problem is even more obvious for liquid water, because water tables require more space for the three variables of x, n and k rather than two variables (x and k) for the ice table. Conservation of computer storage space is more urgent for the water tables, and more efficient design of the tables is thus desired.

Fig. 7 demonstrates that if one integrates a size distribution of particles by a fixed interval ($\triangle r = 50$ μm), the corresponding resolution of x ($\triangle x$) is then solely dependent on the frequency of the incident radiation. This can be readily

understood by the following formula,

$$\triangle x = \frac{2\pi\nu}{c}(\triangle r) \tag{3}$$

where $\triangle r$ is an uniform value ($= 50$ μm in this tabulation) for all frequency channels. The $\triangle x$ needs to be finer at the lower frequencies (longer wavelengths) compared to those at the higher frequencies (shorter wavelengths) in order to integrate Mie quantities on the same resolution of particle size distribution. For instance, $\triangle x = 0.01$ is necessary at 10 GHz frequency in order to reproduce the same accuracy of integrating particle size distributions with $\triangle x = 0.18$ for 180 GHz channel. Let r_{max} be the maximum particle radius corresponding to a different rain rate (RR) obtained by limiting the Marshall-Palmer size distribution to concentration greater than 10^{-10} cm^{-3}. Define x_{max} as the maximum size parameter corresponding to the r_{max}. Apparently, x_{max} is smaller for the lower frequency and larger for the higher frequency channels as shown in Fig. 7. Since the Marshall-Palmer size distribution increases the concentration of larger particles with increasing rain rate, r_{max} and x_{max} obviously will become larger for the higher rain rate. The resolution of x in the table should always be finer than the $\triangle x$, which is related to the x_{max} for each frequency. For a larger x_{max} required in the table, it is more acceptable of having a coarser resolution of $\triangle x$ in the same table. Although the Marshall-Palmer formula may not always be best for describing size distributions of atmospheric cloud and precipitation, the relationship between $\triangle x$ and x_{max} generally has the same tendency as shown in Fig. 7 regardless of the different size distribution being applied.

When x is small, the extended Rayleigh scattering approximation may be accurate enough to simulate the scattering properties. The Rayleigh approximation is only suitable for the scattering by a particle with small absolute value of $m \times x$ (Van de Hulst, 1957). While Van de Hulst developed computations by means of series expansion for small particles, he warned that "aside from their simplicity, they have little advantage. They (the series expansion) describe the very first deviations from Rayleigh scattering, but further deviations appear very soon after the first have become prominent, so that the full Mie formulae have to be used." Wiscombe (1979) also emphasized that the Mie formulae should be used for most of scattering calculations, and only apply the $x \to 0$ formulae over a range of x sufficiently small to avoid serious ill-conditioning but still give six significant digits in all Mie quantities.

In tabulating Mie quantities, we start x as small as 10^{-4}. In view of small magnitudes of extinction and scattering effects of small particles on the overall radiative transfer process, one category of x covering all x smaller than 10^{-3} is given in the Mie table. The Mie quantities for this category are represented by the averaged values calculated for the x between 10^{-4} and 10^{-3}. Results, as will be discussed in the Section 4, indicate that by using the Mie table for small particles, the upwelling brightness temperatures show little discrepancy in comparison with those using Mie calculation in the radiative transfer model.

3. STRUCTURE OF THE TABLE

The average Mie scattering quantities are tabulated from predetermined ranges of size parameter, imaginary and real refractive indices. Appendices A and B show the ranges of x and m for ice and liquid water, respectively. The following sections discuss indepth the procedure for the creation of Mie tables.

The Mie table is constructed by linearly averaging Mie parameters over predetermined ranges of x and m. For liquid water, m includes n and k; but for ice, there are only ranges for k, since n is a constant value. The following steps outline the procedure:

a) Consider a range in size parameter, imaginary and real refractive indices with resolutions of $\triangle x$, $\triangle k$, and $\triangle n$, respectively. For a number of discrete values of size parameters and refractive indices within the ranges, the extinction and scattering efficiency factors and four elements of phase functions are computed. These results are then averaged over the given range. The number of discrete values used for averaging within each range varies for each parameter in different tables; it can be as many as 11 numbers for the x between 18 and 20 in the water table ($>$ 37 GHz), or as few as one for each $\triangle x$ in the ice table.

If V and $\bar{V}$ are the variable to be averaged and the averaged variable, respectively, then

$$\bar{V} = \frac{\left(\sum_{c=1}^{C} \frac{\left[\sum_{b=1}^{B} \frac{\left(\sum_{a=1}^{A} V \right)}{A} \right]}{B} \right)}{C}$$

where

A	:	number of discrete values of x within the predetermined $\triangle x$;
B	:	number of discrete values of k within the predetermined $\triangle k$;
C	:	number of discrete values of n within the predetermined $\triangle n$.

It is more logical and economical to average size parameter first followed by the refractive indices for creating the Mie table. The reason for this approach is explained in section 4.2.

For each predetermined $\triangle x$, $\triangle k$ and $\triangle n$, Mie variables are calculated at several discrete values of x, k, and n. It is found, however, that for ice, because the $\triangle x$ values are very small, only one discrete value of x within $\triangle x$ is necessary to represent the Mie quantities within the range.

b) Before the second step is outlined, it is necessary to understand certain concepts about categories of refractive indices and size parameters. In Tables B.1 and B.3, each category of real refractive indices has one or more categories of imaginary refractive indices. Let $D, E, P, ..., Z$ be the total number of categories of imaginary refractive indices corresponding to each category of real refractive indices. For the purpose of discussion, let us consider S to represent the number of size parameter categories. In Tables A.2, B.2 and B.4, they show that S is 383, 100 and 71 for ice table and water table with frequency $\leq$ 37 GHz and $>$ 37 GHz, respectively. Therefore, the total number of records of the complete water table is $(D + E + ... + Z) \times S$. For ice, since the real refractive index is constant, the total number of categories is $D \times S$.

   For water, the averaging procedure is repeated for size parameter, imaginary refractive index, and real refractive index ranges. For ice, since real refractive index is constant, the averaging procedure is repeated only for size parameter and imaginary refractive index ranges. Table C.1 describes the organization of variables in general. It is more logical and economical to average size parameter first followed by the refractive indices in creating the Mie table. The reason for this approach is explained in Section 4.2.

c) The Mie quantities calculated as a function of refractive index and size parameter are stored in a direct access disk. The main advantage of storing the tables as direct access files is the speed and efficiency with which data can be retrieved. The data are ordered by record number. Any record can be accessed directly without reading other records. A more detailed description of the creation and use of direct access files can be obtained from NASA Space and Earth Sciences Computing Center (NSESCC) publications (1985) and

(1986). These subroutine packages are exclusively for the IBM 3081 MVS operating environment.

3.1 Ice

Complex Refractive Index

Since n is a constant in the microwave region, we only need to consider k in the table. We divide k values into seven categories (see Appendix A), which cover the range of temperature from 10°C to −60°C and frequency from 5 to 300 GHz. The k is very small compared to n, and is limited to a small range. According to the Table II in Warren (1984), the largest k for the frequency and temperature ranges of our interest is 9.54×10^{-3} (at 300 GHz and $T = -1$°C), and the smallest k is 1.73×10^{-4} (at 5 GHz and $T = -60$°C). The resolution of 1×10^{-3} for each category is used in view of slow change of Mie quantities within each $\triangle k$. Fig. 8 depicts the imaginary refractive index of ice as a function of frequency and temperature based on Warren's table. The magnitude of k generally increases with increasing temperature and frequency.

Size Parameter

In the ice table, we have a total of 383 categories of $\triangle x$. Resolution of the first $\triangle x$ is 9×10^{-4} when $x \leq 10^{-3}$, and gradually increases up to 0.4 when $x > 20$. Within each $\triangle x$, the intermediate value of x is used to calculate and represent the Mie quantities in that small region. Because of the fine resolution of $\triangle x$ in the ice table, calculations show that the resulting brightness temperatures are insensitive to the difference of Mie tables being constructed by either one or more discrete points of x within each $\triangle x$. Between 10^{-4} and 22.8 of x, $\triangle x$ has nine different sizes as shown in the Table A.2. The predominant size, which covers from $x = 0.1$ to $x = 4.0$ is $\triangle x = 0.02$. The sharp spikes and rapid oscillations in this region make the upwelling brightness temperatures very sensitive to the resolution chosen for x in the Mie table. It is anticipated that the resolution of x needs to be very fine in order to properly simulate the oscillations. Although $\triangle x$, as depicted in Fig. 7, is a guidance to the resolution required for x in the Mie table, experiments show that such a resolution will make the radiative transfer calculation sensitive to the starting size for the integration of a size spectrum. In the microwave region, if Mie

quantities are calculated directly from Mie codes, integration of size distribution by starting from different sizes (*e.g.* 1 or 25 μm) will make little difference on the results of radiative transfer calculation. The reason for the radiative transfer calculation being sensitive to the starting size of the integration if using the Mie table, is that since the Mie quantities within a $\triangle x$ are represented by one or an averaged set of Mie calculated values within the range, a "phase shift" may result if the starting particle size is varied. In the radiative transfer calculation, the starting size for the integration of size distribution should be set at 25 μm, otherwise, a phase shift of size integration from the Mie table may occur. The effect is more pronounced in the area with sharp spikes. In the experiments using the Wu and Weinman (1984) profile, the phase shift can lead to brightness temperature differences of as much as 6.5 K for 37 GHz, 7.5 K for 85 GHz, and 16.6 K for 183 GHz. The phase shift, however, can be minimized if the resolution of x in Mie table is finer especially in the range of $1 < x < 10$ for ice. Fig. 7 shows that when $x = 4$, $\triangle x$ needs to have a resolution of 0.04 or better. The radiative transfer calculations demonstrate that for $x = 4$, the resolution of x in Mie table needs to be 0.02 (as shown in Table A.2) so that the resulting brightness temperatures are independent of phase shift. This exercise is just to illustrate that in actual tabulation the resolution of x may not be the same as $\triangle x$ of Fig. 7. For $x > 22.8$, both Q_s and Q_e are assumed approaching an asymptotic value; therefore the Mie quantities of the last category of x are used to represent the x beyond 22.8.

Mie Quantities

Besides three input variables of size parameter, real and imaginary indices, three quantities output from the Mie calculations – scattering and extinction efficiency factors and the phase functions, are recorded in the Mie tables. Since a spherical particle is symmetrical with respect to the incident light, the scattering pattern is also symmetrical in the intervals $(0°, 180°)$ and $(180°, 360°)$. The phase functions are, therefore, described by 181 scattering angles including both 0° (forward scattering) and 180° (backward scattering). In tabulating the Mie quantities, we experimented averaging phase angles in order to save computer storage space without impacting the accuracy of the Mie table. In Fig. 9, an example of the first two phase functions of scattering by the ice particles is shown, and in Fig. 10, the two-degree averaging of the scattering angles for the same case is shown. The minor differences due to the angle averaging do not significantly affect the results

of radiative transfer calculations. In Table 2, results of the brightness temperatures are compared for different number of scattering angles being used in the radiative transfer calculation. The 181 represents the full phase functions being calculated by every scattering angle from 0° to 180°; 90 and 60 represent the phase functions being averaged for every 2 and 3 degrees, respectively. Results show that the two-degree averaging of phase angles, in general, has an excellent agreement with the full calculation of every phase angle; the maximum discrepancy is 0.8 K at 85.5 GHz. The discrepancy for three-degree averaging exceeds 18 K for 183 GHz; this obviously can not satisfy the required accuracy for the tables. In the Mie table for ice, we average phase functions for every two degrees of scattering angle, and save about a factor of two of computer storage space.

3.2 Liquid Water

For liquid water, the Mie tables are divided into two parts; the first part is for the frequencies less than and including 37 GHz, and the other part is for the frequencies greater than 37 GHz. The reasons for breaking the table into two parts are:

(a) The low frequencies ($5 \leq \nu \leq 37$ GHz) need to have a finer resolution of x but have a smaller x_{max} in the tables; on the contrary, the high frequencies ($37 > \nu > 300$ GHz) need a larger x_{max} but a coarser resolution; and

(b) the phase functions behave quite differently for the low and high frequencies; division of the Mie tables in two parts saves significant computer storage space.

Complex Refractive Index

Since n and k are not directly related to each other for all temperatures and frequencies, we need to treat n and k as two independent variables. Two important factors that should be considered for this tabulation are: (a) only the ranges of m which actually occur in the realistic atmosphere will be tabulated, and (b) the resolution of m in the table depends on the sensitivity of the Mie solutions to the variation of m. Fig. 11 shows that the Mie quantities change much more quickly for smaller real and imaginary refractive indices (higher frequency) than for larger refractive indices (lower frequency). Therefore, we should tabulate more detailed

Mie results in the region of smaller m than in those of larger m. The shaded areas in Fig. 11, like Figs. 3 and 4, indicate those complex refractive indices will not exist in the real atmosphere. We intentionally permit a wider range of m (unshaded area in Fig. 11) to be included in the table, because any formula different from Ray (1972) or Lane and Saxton (1952) for computing m may stretch n or k out of the envelopes of the curves as shown in Figs. 3 and 4. However, we do not expect any new formula would produce curves dramatically different from those shown in Figs. 3 or 4.

The sensitivity of Mie results on m is closely related to the x value. Fig. 9b shows that the values of extinction efficiency factor are strongly dependent on the change of m value at $x = 0.72$, while such a dependence is much less obvious for $x = 0.22$ and 3.20 (Fig. 11a and c, respectively). Our experiments reveal that when $x = 0.72$, the Mie quantities are most strongly dependent on the variation of the complex refractive index. Such a dependence is weaker when x either increases or decreases from 0.72. 'Based on Fig. 11b, it appears that the Mie quantities change more rapidly in the region of smaller n (high frequency). However, as shown in Fig. 3, the values of n in the high frequency part distribute over a smaller range ($1.5 < n < 6$) compared to those in the low frequency part ($2 < n < 9$). We tabulate n in 12 categories for the high frequency part, and 22 categories for the low frequency part. For each category of n, the number of k is dependent on (a) resolution of k which is needed to accurately describe the Mie results, and (b) range of k which is needed to cover the designated frequency and temperature ranges. The number of categories and resolution of n and k in each category of n are listed in Tables B.1 and B.3 for the low and high frequency parts, respectively, in the Appendix B.

For each category of n and k, the number of discrete values used for the averaging is varied dependent on the resolution of $\triangle n$ and $\triangle k$. For both low and high frequency tables, the resolution of the discrete values of n and k used for averaging is fixed at 0.1, so more discrete values are used for larger $\triangle n$ or $\triangle k$, and vice versa. For low frequency table, up to eight discrete values of k are used for averaging within a range (*e.g.* $k = 1.7 \sim 2.4$ for $n = 8.1 \sim 8.4$), and $\triangle n$ is uniformly represented by four discrete values in each range. For the high frequency water table, eight discrete values of n ($5.5 \sim 6.2$) are required for averaging, but only up to six of dicrete points of k are used for averaging to represent $\triangle k$.

Size Parameter

For liquid water, both the ripples and major maxima and minima of Mie scattering for an ice particle are mostly damped out due to strong absorption in liquid phase (see Fig. 6). The resolutions of x in the water tables thus are not required to be as fine as those in the ice table.

Two different sets of size parameter are given in the water tables for the low and high frequency channels, as shown in Tables B.2 and B.4, respectively, in the Appendix B. A total of 100 categories of x are given for the low frequency part. The averaged Mie solutions in the first category of x, covering $1 \times 10^{-4} \sim 5 \times 10^{-4}$, also represent the Mie solutions for x smaller than 1×10^{-4}. This approximation does not significantly affect the accuracy of the Mie tables used in the radiative transfer calculations, as will be discussed in the next section. For high frequency part, a total of 71 categories of x are given. In the tables, although the Mie solutions for both the low and high frequency parts are tabulated from the same x (1×10^{-4}), the maximum x in the low frequency part is only 5, while the maximum x in the high frequency part extends to 20. The resolution for x in the low frequency part is much finer than that in the high frequency part. The Mie solutions for the last categories of x are used for any x greater than x_{max} in the tables. This approximation is based on (a) x is unlikely to be larger than x_{max} in the microwave region, and (b) the Mie solutions usually approach asymptotic values after x exceeds x_{max}.

Mie Quantities

The phase functions of the low frequencies are generally quite smooth with respect to the scattering angles (*e.g.* Fig. 12 for $x = 1$ at 37 GHz and 0°C); so the phase functions can be averaged over every nine degrees without seriously affecting the results. In Fig. 13, an example of the phase function one and two of scattering by liquid water droplets for $x = 4$ at 18 GHz is shown. The curves in Fig. 13 are less linear than those in Fig. 12, because the scattering pattern at $x = 4$ is less uniform compared to that at $x = 1$. In fact, the case of $x = 4$ shows the least smooth phase functions in the low frequency part of the table ($x \leq 5$). By averaging every nine degrees of the phase angles, the phase functions are shown (in Fig. 15) as step functions. Although the patterns of phase function for 18 and 90 GHz are quite similar for the same x (see Fig. 13 and 15), their magnitudes are different due to the difference of their complex refractive indices. The phase functions of 18 GHz would

look smoother if the scale used for 90 GHz were used. Our experiments indicate that for the high frequency channels, averaging every two degrees (Fig. 16) is necessary to insure an accurate Mie table. Table 3 shows that the difference between results of full resolution (181 angles) and two, three and nine degrees averaging (90, 60, and 20 angles, respectively) of phase functions. The table should be divided into two parts: the low frequency channels generally have excellent comparison between full resolution values and values based on nine degree averaging of the phase functions, but the high frequency channels (> 37 GHz) only show a good comparison with two degree averaging. Since the phase functions occupy most of the disk space in the Mie tables, the nine degree averaging of phase angles saves the computer storage space by about a factor of nine and two degree averaging by a factor of two.

4. RESULTS AND DISCUSSION

4.1 Comparison of Results from Mie Tables and Mie Calculations

The microwave radiative transfer model, used for testing the accuracy and efficiency of the Mie tables, is based on the model described by Szejwach *et al.* (1986), which is a revised model of Wilheit it et al. (1982). The revised model includes the capability of handling up to 200 atmospheric layers and 19 regions for cloud and precipitation; each region allows up to 4 classes of mixed-phase hydrometeors including water and ice cloud, raindrop and graupel. The input Mie quantities for calculation of the scattering effect in the radiative transfer simulation will be obtained directly from Mie tables. The upwelling microwave brightness temperatures resulting from this radiative transfer calculation will be compared with those brightness temperatures using Mie quantities obtained from the computation of Mie codes. The profile selected for the initial comparison is based on that used by Wu and Weinman (1984), and further evaluation is performed by comparing results of 144 atmospheric profiles generated by Tao's three-dimensional cloud model (Tao, 1986) in simulation of a tropical convective system during the GARP (Global Atmospheric Research Program) Atlantic Tropical Experiment (GATE).

For the initial comparison, the calculations are divided into two parts; one is the atmospheric profile with ice (cloud ice and graupel) only, and the other is the profile with liquid water (cloud water and rainwater) only. Finally, we will combine both phases to assess the Mie table.

Ice Table

It is important to first test one phase only, because by assuming no liquid water in the profile, the scattering from ice will not be influenced by strong absorption of liquid water. The brightness temperatures are computed based on the Wu and Weinman profile (see Fig. 1) for $RR = 64$ mm/hr over land. Results of the upwelling brightness temperatures at 50° zenith angle by using the Mie table (Appendix A) are compared with those Mie quantities calculated by the subroutine

DBMIE (Mie codes). In Table 4, the comparisons show that the worst discrepancy is 1.1 K at 183 GHz, which is the frequency most sensitive to the presence of ice among frequencies listed for the comparisons. Figs. 17a and b show an example of the Mie quantities calculated from the Mie codes and directly obtained from the ice table, respectively. Both diagrams are plotted with a resolution of $x = 0.2$ and show the resemblance with only slight differences appearing in the region of x between $4 \sim 8$. The maximum discrepancy of the extinction coefficients appears at $x = 6$ with less than 5% difference.

Water Tables

For cases with liquid water only in the profile, the ice content is assumed to be zero and liquid water content is distributed as shown in Fig. 1 for $RR =$ 64 mm/hr case. Results of the upwelling brightness temperature are shown in the Table 5 with the worst discrepancy of 1.3 K occurring at 85.5 GHz. This may be due to coarser resolution of x in the Mie table when x becomes larger (Table B.3). Since the peak absorption of water vapor at 183 GHz is in the upper atmosphere (above 300 mb), lower clouds with liquid water only may not have a strong effect on the upwelling brightness temperatures as high cloud with abundance of ice. Fig. 18a and b show the Mie quantities calculated from the Mie codes and directly obtained from the water table, respectively. Since the maximum difference of the Mie quantities between Figs. 11a and b are no more than 1% (at $x = 1.2$), one can hardly identify the difference between the two diagrams.

Combination of Ice and Water Tables

After separately assessing the ice and water tables, we then calculate the upwelling brightness temperatures for a mixed phase profile (Fig. 1) with $RR = 64$ by using both ice and water tables for the scattering properties in the cloud and precipitation regions. Results are compared with the brightness temperatures using the Mie codes to compute the scattering parameters for the same case. As shown in Table 6, the worst comparison is at 85.5 GHz with a discrepancy of 1.3 K. At 183 GHz, the comparison shows the discrepancy to be merely -0.1 K. This may be due to the compensation from the bias of ice (-1.1 K) and water (0.5 K), which makes comparison of the mixed phase profile more favorable. This "compensation

effect" does not appear to other frequencies for this particular profile. In fact, both ice and water tables show excellent agreement at 37 GHz (Tables 4 and 5), but the combination of the two phases results in large discrepancy as shown in Table 6. It is interesting to see that under any of the tested conditions, the Mie tables always give excellent results for the lower frequencies (< 37 GHz).

Bias and RMS Deviations of 144 Profiles

To prove the Mie table is valid for a wide range of frequency, temperature, ice and water concentrations, a statistical comparison of brightness temperature (T_b), obtained by a direct Mie calculation (subroutine DBMIE) and by using Mie table is required. The bias and RMSD can be defined as :

$$bias = \frac{\left(\sum_{i=1}^{N} T_{b,i}\right)}{N}$$

$$RMSD = \left(\frac{\sum_{i=1}^{N} (T_{b,i} - bias)^2}{N} \right)^{1/2}$$

where

$T_{b,i}$	:	$T_{b,Table} - T_{b,DBMIE}$,
N	:	sample population.

A sample of 144 profiles was selected from a three-dimensional cloud model (Tao, 1986). This model can be run in two or three dimensions, although present computing capacity permits only a rather restricted domain for the three-dimensional runs. It can also be run with two or three classes of ice. With two ice classes, the bulk parameterization is similar to that for water droplets, with small "cloud ice" particles having little or no terminal velocity and the larger-sized graupel or hail category falling relative to the air. The third, or intermediate size class of ice (snow) proves to be essential in capturing key features of tropical clouds. It has a finite terminal velocity, but one which is much less than that of graupel. A comparison of the substantial differences between the ice parameterizations in use has been made by McCumber *et al.* (1987) by trying several of these in the multi-cloud model. So far, the scheme by Rutledge and Hobbs (1984) appears to give a realistic bright

melting band and anvil precipitation in the GATE cases (Simpson *et al.* , 1988). Fig. 19 shows rain rate results from a three-dimensional run with this ice parameterization, using the same environment observed for fast-moving squall lines in the GATE. The square drawn in the figure is a 12×12 grid box covering 18 km $\times$ 18 km area (with resolution of 1.5 km). There are many different combination of hydrometeors resulted from the cloud model simulation in this area. It appears that this is an ideal region for testing the Mie tables.

The brightness temperatures (vertical and horizontal polarizations) were obtained from the radiative transfer model using the Mie table and subroutine DBMIE for several viewing angles and frequencies. Table 7 illustrates the bias and RMSD values. For the 144 profiles generated from the cloud model, comparisons indicate that 37 and 90 GHz have larger discrepancies than 183 GHz. For more general cases, the water vapor absorption may smear out some of the scattering effect from ice and make the comparison more favorable at 183 GHz. The 90 GHz has the largest RMSD of 1.65 K at nadir angle and the maximum absolute discrepancy of 3 K. The brightness temperatures calculated based on the Mie table mostly are overestimated except those at 10 and 174 GHz. The overestimation may be because the Mie tables tend to smooth out the rapid oscillations of the Mie scattering, especially for ice particles. The "smooth effect" may cut out some of the scattering effect and increase the upwelling brightness temperatures. Over all, the comparison is quite satifactory with the maximum bias and RMSD of merely 1.7 K. The comparisons reveal that the Mie tables indeed may replace the Mie calculations in the microwave radiative transfer modeling simulation without seriously sacrificing the accuracy of the modeling results.

4.2 Timing and Cost Analysis

The two factors that affect the cost of a computer calculation are the TIME and the number of EXCP (EXecute Channel Programs) (see NSESCC publication, 1985). The TIME operand gives the total amount of processing time for the job including all steps. The EXCP refers to the number of input/output operations performed.

In section 3 it was noted that tabulating Mie quantities by averaging size parameter first is more logical and economical. In radiative transfer models we

compute the complex refractive index first, based on the frequency and the prevailing temperature of the region. Then for each region, and for each set of particle size distribution, the sequential size parameter is computed. In other words, we have a spectrum of particles in each region, with a complex refractive index and size parameter, for which the extinction and scattering efficiency factors and phase functions are required. By organizing the Mie table in this fashion, the Mie parameters from the table can be accessed as a block for a spectrum of particles in a region, thereby reducing the number of EXCP. As a test, we also accessed the tabulated results one size parameter at a time, for each region. The number of EXCP was approximately 13 and 4 times larger at 10 and 183 GHz, respectively.

Table 8 compares the total CPU time and the number of EXCP, for 144 profiles, using the Mie calculation (DBMIE) and the Mie table. The use of Mie table reduces the CPU time by a factor of 7 at 10 GHz, increasing to a factor of 16 at 183 GHz. The use of Mie table, however, increases the number of EXCP. The large EXCP at the high frequencies simply reflects the fact that more size parameters are accessed from the Mie table. Table 9 lists the percentage saving in cost calculated for the IBM 3081 (Batch) using Mie table compared to using Mie calculation. When the Mie table is used, the saving in time is somewhat offset by increase in the number of EXCP. Overall, the cost saving varies from 83% to 89% or a factor of 6 to 9.

In section 3 it was noted that tabulating Mie quantities by averaging the size parameter first is more logical and economical. In radiative transfer models we compute the complex refractive index first, based on the frequency and the prevailing temperature of the region. Then for each region, the sequential size parameters are computed. In a block of the Mie table, if the Mie quantities are tabulated in the sequence starting from the smallest to the largest size parameters, the table can be accessed as a block for a spectrum of particles in a region, thereby reducing the number of EXCP. As a test, we also accessed the Mie tables one size parameter at a time, for each region. The number of EXCP was approximately 13 and 4 times larger at 10 and 183 GHz, respectively.

5. SUMMARY:

The purpose of tabulating the Mie tables is to save computer time for microwave radiative transfer model simulation, which consumes large portion of CPU time for Mie calculations. Comparisons between the upwelling brightness temperatures based on the Mie tables and the Mie calculations reveal that the Mie tables may indeed replace the Mie calculations in the microwave region. In an experiment of testing 144 profiles with various combinations of ice and liquid water, we found that the bias and RMSD of the upwelling brightness temperatures by using the Mie tables are less than 1 K for $10 \sim 183$ GHz except at 37 and 90 GHz. The overall comparisons show that the maximum bias and RMSD have not exceeded 1.7 K.

Although the efficiency improvement by using the Mie tables in the microwave radiative transfer calculations have been encouraging, there are still some revisions of the current Mie tables that can be done to further improve the efficiency without affecting the accuracy.

(1) It is important to further reduce computer storage space needed for the Mie tables, if one considers running a microwave radiative transfer model in a computer system with much limited disk space. It is possible to further reduce size of the ice table without affecting the accuracy of using the Mie tables in the microwave radiative transfer calculations. Since the absorption of ice in the microwave region is weak, the scattering and extinction properties of ice (see Figs. 20 and 21, respectively, for 90 GHz) are thus weakly dependent on the temperature and frequency variations. The corresponding first phase functions for 90 GHz, which are plotted for a series of size parameter as shown in Figs. 22a and b for 0°C and −50°C, respectively, show their resemblance. Both diagrams have a very similar pattern indicating that the first phase function is not strongly dependent on temperature variations. Figs. 23a and b depict the second phase functions, which are also weakly associated with the temperature variations. Since the complex refractive index is a function of both temperature and frequency, it is also important to examine the Mie quantities with respect to the frequency changes. Figs. 24a and b show the first phase functions of 18 GHz at 0°C and −50°C, respectively. By comparing Figs. 22 and 24 (90 versus 18 GHz for the first phase function), and 23 and 25 (for the second phase function), we may conclude that the Mie quantities, especially the

phase functions change slowly with respect to the imaginary refractive index (real refractive index is constant). Since the phase functions occupy the majority of the computer storage space in the Mie tables, it is feasible to share each set of phase functions by a wider range of complex refractive index. The savings in computer storage is expected to be significant. If every two categories of complex refractive index in the current Mie tables share one set of phase functions, almost one half of the computer storage space can be eliminated for the ice table.

(2) The phase functions in the current Mie tables are tabulated as function of scattering angles. It is desirable to also represent the phase function in term of the Legendre moments, so the Mie tables can be more widely useful for different microwave radiative transfer models. This modification may not neccessarily save computer storage space for the Mie tables, because many phase functions need more than 100 terms of the Legendre moments in order to accurately describe the scattering pattern. Although it is likely to have some phase functions represented by just a few terms of the moments, there may be technical difficulties in having variable record length in the computer storage space.

(3) The discrepancy between the Mie tables and the Mie calculations is expected to further reduce if the resolution of the size parameter in the tables can be increased. This is particularly important for the ice table, because the rapid oscillations of the scattering and extinction properties as a function of the size parameter are evident in the scattering by ice.

6. REFERENCES:

Asano, S., and M. Sato, 1980: Light scattering by randomly oriented spheroidal particles. Appl. Opt., 19, 962-974.

Cole, K.S., and R.H. Cole, 1941: Dispersion and absorption in dielectrics. I: Alternating current characteristics. J. Chem. Phys. 9, 341-351.

Champion, P.M. and A.J. Sievers, 1980: Far infrared magnetic resonance of deoxyhemoglobin and deoxymyoglobin. J. Chem. Phys, 72, 1569-1582.

Cumming, J., 1952: The dielectric properties of ice and snow at 3.2 cm. J. Applied Phys., 23, 768-779.

Evans, S., 1965: Dielectric properties of ice and snow – A review. J. Glaciol., 773-792.

Heymsfield, A.J., 1986: Ice particle evolution in the anvil of a severe thunderstorm during CCOPE. J. Atmos. Sci., 43, No. 21, 2463-2478.

Jacobowitz, H., 1971: A method for computing the transfer of solar radiation through clouds of hexagonal ice crystals. J. Quant. Spectr. Rad. Trans., 11, 691-695.

Knight, R.J. and D.T. Llewellyn-Jones, 1984: Measurement of the complex refractive index of sea ice and snow using a microwave untuned cavity. Report RAL-84-093, Rutherford Appleton Laboratory, Chilton, Didcot, Oxon, OX11 0QX.

Lane, J.A., and J.A. Saxton, 1952: Dielectic dispersion in pure polar liquids at very high radio-frequencies, I. Measurements on water, methyl and ethyl alcohols. Proc. Royal Soc. (London) 213, 400-408.

Liou, K.N., Q. Cai, P.W. Barber, and S.C. Hill, 1983: Scattering phase matrix comparison for randomly hexagonal cylinders and spheroids. Appl. Opt., 22, No. 11, 1684-1687.

McCumber, M.C., W.-K. Tao, J. Simpson, R. Penc and S.T. Soong, 1987: Compari-

son of ice-phase microphysical parameterization schemes in tropical, fast-moving convective line simulations. Preprint Vol. 17th Conf. Hurricanes Tropical Meteor., Amer. Meteor. Soc., Miami, FL, April 1987.

NASA Space and Earth Sciences Computing Center, 1985: Introduction to NSESCC JCL, Document number SESC - UG05 - 04, NASA / GSFC, 141 pp.

NASA Space and Earth Sciences Computing Center, 1986: FTIO and DAIO subroutine packages, Document number SESC - UG15 - 01, NASA / GSFC, 103 pp.

Ray, P. S., 1972: Broadband complex refractive indices of ice and water. Appl. Opt., 11, 1836-1844.

Rutledge, S.A. and P.V. Hobbs, 1984: The mesoscale and microscale structure and organization of clouds and precipitation in midlatitude clouds. Part XII: A diagnostic modeling study of precipitation development in narrow cloud frontal bands. J. Atmos. Sci., 41, 2949-2972.

Simpson, J., R.F. Adler and G.R. North, 1987: On some aspects of a proposed tropical rainfall measuring mission (TRMM). Bull. Amer. Meteor. Soc. (Submitted).

Szejwach, F., R.F. Adler, I. Jobard, and R.A. Mack, 1986, Preprint Vol. 2nd Conf. Sat. Meteor./Rem. Sens. Appl., Amer. Meteor. Soc., Williamsburg, VA., May, 1986.

Tao, W. -K., and S. -T. Soong, 1986: The study of the response of deep tropical clouds to mesoscale processes: Three-dimensional numerical experiments. J. Atmos. Sci., 43, 2653-2676.

Van de Hulst, H. C., 1957: *Light Scattering by Small Particles.* John Wiley & Sons, Inc.,N.Y., p. 271.

Warren, S.G., 1984: Optical constants of ice from the ultraviolet to the microwave. Appl. Opt., 23, 1206-1225.

Weinman J.A., and P.J. Guetter, 1977: Determination of rainfall distribution from microwave radiation measured by the Nimbus 6 EMSR. J. Appl. Meteor.,

Wilheit, T.T., A.T.C. Chang, J.L. King, E.B. Rodgers, R.A. Nieman, B.M. Krupp, A.S. Milman, J.S. Stratigos, and H. Siddalingaiah, 1982: Microwave radiometric observations near 19.35, 92 and 183 GHz of precipitation in tropical strom Cora. J. Appl. Meteor., 21, 1137-1145.

Willis, P.T., 1984: Functional fits to some observed drop size distribution and parameterization of rain. J. Atmos. Sci., 41, No. 9, 1648-1661.

Wiscombe, W., 1979: Mie scattering calculations: Advances in technique and fast, vector-speed computer codes. NCAR Technical Note, NCAR/TN-140+STR, p. 81.

Wiscombe, W.J., 1980: Improved Mie scattering algorithms. Appl. Optics, 19, 1505-1509.

Worz, O., and R.H. Cole, 1969: Dielectric paroperties of ice I. J. Chem. Phys., 51, 1546-1531.

Wu, R. and J.A. Weinman, 1984: Microwave radiances from precipitating clouds containing aspherical ice, combined phase, and liquid hydrometeors. J. Geophys. Res., 89, D5, 7170-7178.

Yeh, H.-Y. and K.-L. Liou, 1983: Remote sensing of cloud parameters from a combination of infrared and microwave channels. J. Cli. Appl. Meteor., 22,, No. 2, 201-213.

Yeh, H.-Y. M., M.-L. C. Wu, and R.J. Curran, 1983: Experiment on the retrieval of cloud parameters from the AMMS and MCR data. Preceeding Fifth Conf. Atmos. Rad., AMS, Oct. 31- Nov. 4, 1983, Baltimore, MD.

Zerull, R.H., 1976: Scattering measurements of dielectric and absorbing nonspherical particles. Beitr. Phys. Atmos., 49, 166-188.

Table 1. CPU time for Mie calculation in the radiative transfer model using Wu and Weinman (1984) (64 mm/hr) profile.

Frequency (GHz)	Number of times DBMIE was called	CPU time for Mie calculation (sec)	Total CPU time (sec)	Percentage of total CPU time used for Mie calculation
6.6	2068	28.0	37.0	76
10.7	2068	28.0	40.6	69
18.0	2068	33.0	44.9	73
37.0	2068	43.0	53.6	80
183.0	2068	89.0	103.0	86

Table 2. Comparison of brightness temperatures (K) by using various number of angles describing phase function in the model simulation. The atmospheric profile is based on Wu and Weinman (1984) with rainfall rate of 64 mm/hr for ice only filling entire cloud regions. The viewing angle is 50 degrees from nadir and surface emissivity = 0.5.

Frequency (GHz)		Number of angles in the phase functions		
		181	90	60
6.6	(V)	153.8	153.8	153.8
	(H)	153.8	153.8	153.8
10.7	(V)	155.6	155.6	155.6
	(H)	155.5	155.5	155.5
18.0	(V)	163.6	163.6	163.6
	(H)	163.0	163.0	163.1
21.0	(V)	179.8	179.8	179.8
	(H)	178.7	178.7	178.8
37.0	(V)	104.1	104.0	104.6
	(H)	104.7	104.6	105.3
85.5	(V)	64.9	65.7	74.2
	(H)	65.0	65.8	74.4
183.0	(V)	78.4	78.8	96.8
	(H)	78.2	78.7	96.7

Table 3. Same as Table 2 except liquid water only.

Frequency (GHz)		Number of angles in the phase functions			
		181	90	60	20
6.6	(V)	270.4	270.4	270.4	270.4
	(H)	270.0	270.0	270.0	270.0
10.7	(V)	261.0	261.0	261.0	261.0
	(H)	260.1	260.1	260.1	260.1
18.0	(V)	246.1	246.1	246.1	246.2
	(H)	244.7	244.7	244.7	244.8
21.0	(V)	242.9	242.9	242.9	242.9
	(H)	241.3	241.3	241.3	241.5
37.0	(V)	235.7	235.6	235.8	236.0
	(H)	233.7	233.7	233.8	234.1
85.5	(V)	235.4	235.2	236.0	238.4
	(H)	233.9	233.8	234.6	237.3
183.0	(V)	239.1	238.9	240.5	246.9
	(H)	238.9	238.8	240.4	247.1

Table 4. Brightness temperatures (K) computed based on ice table for Wu and Weinman (1984) 64 mm/hr (ice only) profile. DBMIE indicates brightness temperatures calculated using Mie code. Surface emissivity = 0.9.

Frequency	Vertical			Horizontal		
(GHz)	DBMIE	Table	Table-DBMIE	DBMIE	Table	Table-DBMIE
6.6	268.5	268.5	0.0	268.5	268.5	0.0
10.7	265.6	265.6	0.0	265.6	265.6	0.0
18.0	246.2	246.2	0.0	245.9	245.9	0.0
21.0	232.3	232.4	0.1	231.9	232.0	0.1
37.0	127.9	127.8	-0.1	129.1	129.0	-0.1
85.5	62.2	62.4	0.2	62.3	62.5	0.2
183.0	77.7	76.6	-1.1	77.6	76.5	-1.1

Table 5. Brightness temperatures (K) computed based on water tables for Wu and Weinman (1984) 64 mm/hr (liquid water only) profile. Surface emissivity = 0.9.

Frequency	Vertical			Horizontal		
(GHz)	DBMIE	Table	Table-DBMIE	DBMIE	Table	Table-DBMIE
6.6	272.7	272.9	0.2	272.4	272.7	0.3
10.7	256.6	256.7	0.1	256.0	256.1	0.1
18.0	241.4	241.6	0.2	240.2	240.3	0.1
21.0	238.0	238.3	0.3	236.6	236.8	0.2
37.0	230.4	230.5	0.1	228.5	228.6	0.1
85.5	227.9	229.2	1.3	226.5	227.7	1.2
183.0	232.0	232.5	0.5	231.7	232.3	0.6

Table 6. Brightness temperatures (K) computed using both ice and water tables for Wu and Weinman (1984) 64 mm/hr (liquid water + ice) profile. Surface emissivity = 0.9.

Frequency	Vertical			Horizontal		
(GHz)	DBMIE	Table	Table-DBMIE	DBMIE	Table	Table-DBMIE
6.6	272.4	272.4	0.0	272.2	272.2	0.0
10.7	255.0	255.2	0.2	254.4	254.6	0.2
18.0	231.2	231.4	0.2	229.4	229.6	0.2
21.0	222.1	222.2	0.1	220.1	220.2	0.1
37.0	163.3	164.9	0.6	161.8	163.4	1.6
85.5	84.5	85.8	1.3	84.5	85.7	1.2
183.0	84.9	84.8	-0.1	84.8	84.7	-0.1

Table 7. Bias and RMS error of brightness temperatures (K) in using Mie tables.

Frequency (GHz)	Viewing angle (degrees)	Bias		RMS error	
		Vertical	Horizontal	Vertical	Horizontal
10	94.5	0.110	0.050	0.762	0.867
	103.5	0.075	-0.015	0.371	0.472
	112.5	0.030	-0.048	0.303	0.372
	121.5	-0.008	-0.066	0.343	0.384
	130.5	-0.031	-0.073	0.395	0.406
	139.5	-0.054	-0.087	0.419	0.435
	148.5	-0.067	-0.088	0.443	0.437
	157.5	-0.079	-0.084	0.449	0.455
	166.5	-0.088	-0.087	0.449	0.450
	175.5	-0.090	-0.081	0.448	0.452
18	94.5	0.105	0.083	0.273	0.276
	103.5	0.129	0.148	0.204	0.263
	112.5	0.160	0.183	0.181	0.260
	121.5	0.175	0.198	0.176	0.253
	130.5	0.188	0.217	0.185	0.242
	139.5	0.204	0.236	0.190	0.230
	148.5	0.206	0.239	0.196	0.228
	157.5	0.212	0.239	0.206	0.222
	166.5	0.205	0.235	0.208	0.218
	175.5	0.210	0.236	0.206	0.214
37	94.5	1.277	1.212	0.972	0.866
	103.5	1.319	1.317	1.026	0.925
	112.5	1.379	1.347	0.976	0.881
	121.5	1.387	1.334	0.937	0.848
	130.5	1.325	1.346	0.853	0.809
	139.5	1.370	1.394	0.867	0.820
	148.5	1.342	1.392	0.836	0.806
	157.5	1.339	1.371	0.818	0.789
	166.5	1.294	1.351	0.805	0.787
	175.5	1.312	1.378	0.825	0.801
90	94.5	0.801	0.770	0.994	1.001
	103.5	0.889	0.899	1.103	1.104
	112.5	1.126	1.105	1.236	1.237
	121.5	1.200	1.145	1.338	1.342
	130.5	1.106	1.124	1.433	1.425
	139.5	1.284	1.272	1.495	1.494
	148.5	1.398	1.408	1.599	1.595
	157.5	1.284	1.266	1.596	1.598
	166.5	1.233	1.238	1.624	1.624
	175.5	1.375	1.371	1.653	1.653

Table 7. (continued)

Frequency (GHz)	Viewing angle (degrees)	Bias		RMS error	
		Vertical	Horizontal	Vertical	Horizontal
120.6	94.5	-0.021	-0.045	0.165	0.164
	103.5	0.022	0.023	0.163	0.161
	112.5	0.248	0.224	0.178	0.177
	121.5	0.229	0.173	0.182	0.179
	130.5	0.089	0.099	0.188	0.190
	139.5	0.246	0.230	0.204	0.204
	148.5	0.386	0.394	0.215	0.215
	157.5	0.189	0.170	0.217	0.215
	166.5	0.097	0.102	0.223	0.224
	175.5	0.274	0.271	0.218	0.219
174	94.5	-0.609	-0.629	0.513	0.507
	103.5	-0.657	-0.658	0.528	0.532
	112.5	-0.410	-0.431	0.527	0.521
	121.5	-0.553	-0.594	0.571	0.558
	130.5	-0.760	-0.767	0.574	0.580
	139.5	-0.723	-0.738	0.627	0.623
	148.5	-0.430	-0.430	0.562	0.563
	157.5	-0.834	-0.845	0.639	0.633
	166.5	-0.996	-0.997	0.667	0.669
	175.5	-0.699	-0.702	0.616	0.616
183	94.5	0.078	0.058	0.081	0.061
	103.5	0.092	0.084	0.088	0.073
	112.5	0.288	0.274	0.238	0.221
	121.5	0.197	0.172	0.158	0.141
	130.5	0.105	0.104	0.107	0.097
	139.5	0.165	0.157	0.127	0.121
	148.5	0.311	0.313	0.259	0.257
	157.5	0.122	0.115	0.106	0.103
	166.5	0.045	0.045	0.063	0.063
	175.5	0.188	0.186	0.161	0.160

Table 8. Total CPU time and EXCP for executing radiative transfer model for 144 profiles.

Frequency (GHz)	Total CPU time (Min)		Total EXCP	
	Mie calculation	Mie table	Mie calculation	Mie table
10	71.4	10.1	1099	7,818
18	82.1	11.4	1104	9,485
37	101.6	12.9	1101	15,679
90	145.0	17.3	1091	28,772
120.6	164.6	17.3	1113	34,243
174	199.2	16.6	1116	38,283
183	200.9	12.7	1115	38,985

Table 9. Cost analysis, based on NASA Space and Earth Sciences Computing Center computing unit accrual table, fiscal year 1987 (Table C.3), for 144 profiles.

Frequency (GHz)	% Saving in using Mie table over Mie calculations
10	83.2
18	83.3
37	83.3
90	83.3
120.6	84.4
174	87.0
183	89.0

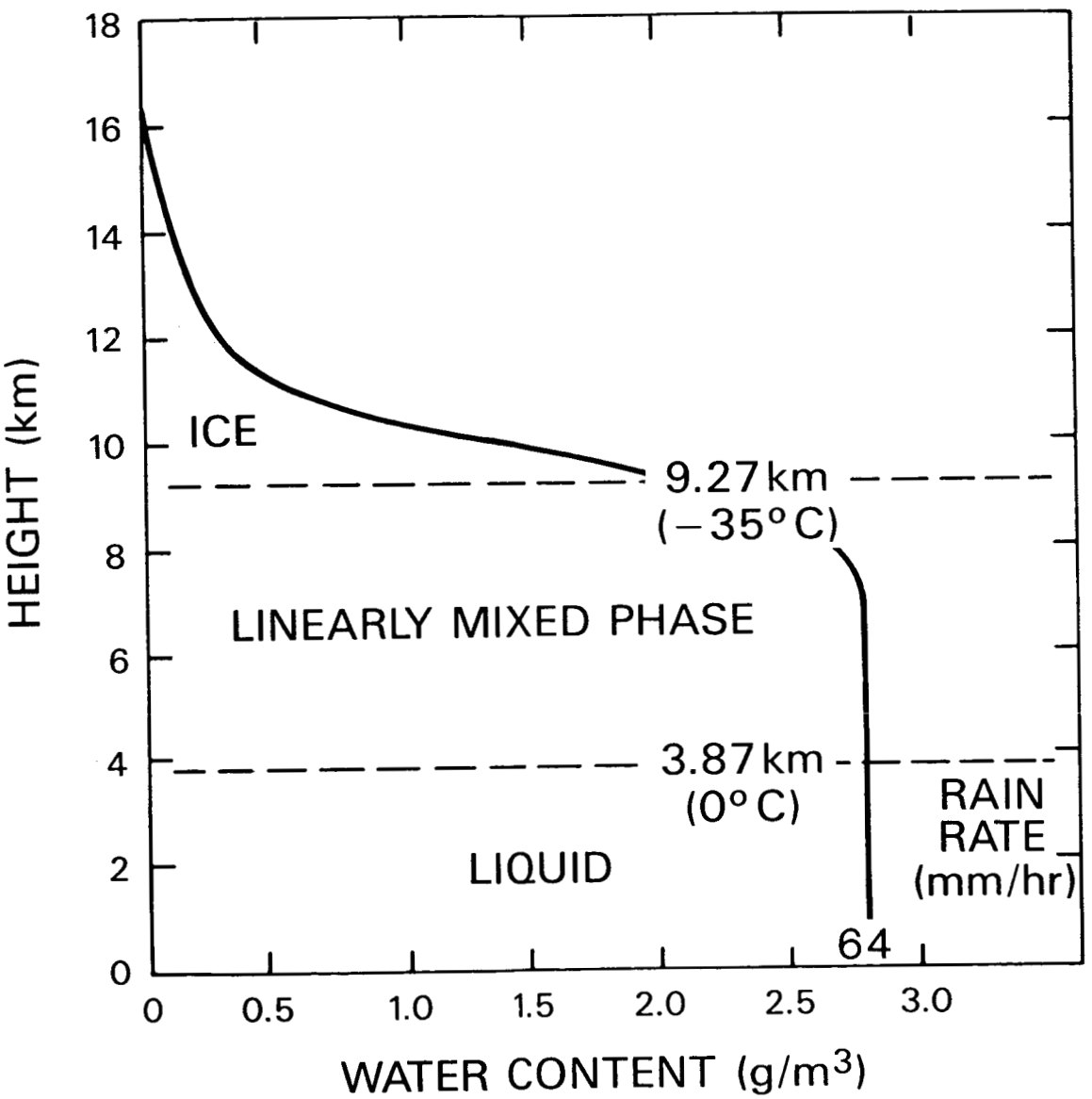

Fig. 1. Schematic model of the distribution of hydrometeors with various phases as a function of height (from Wu and Weinman, 1984).

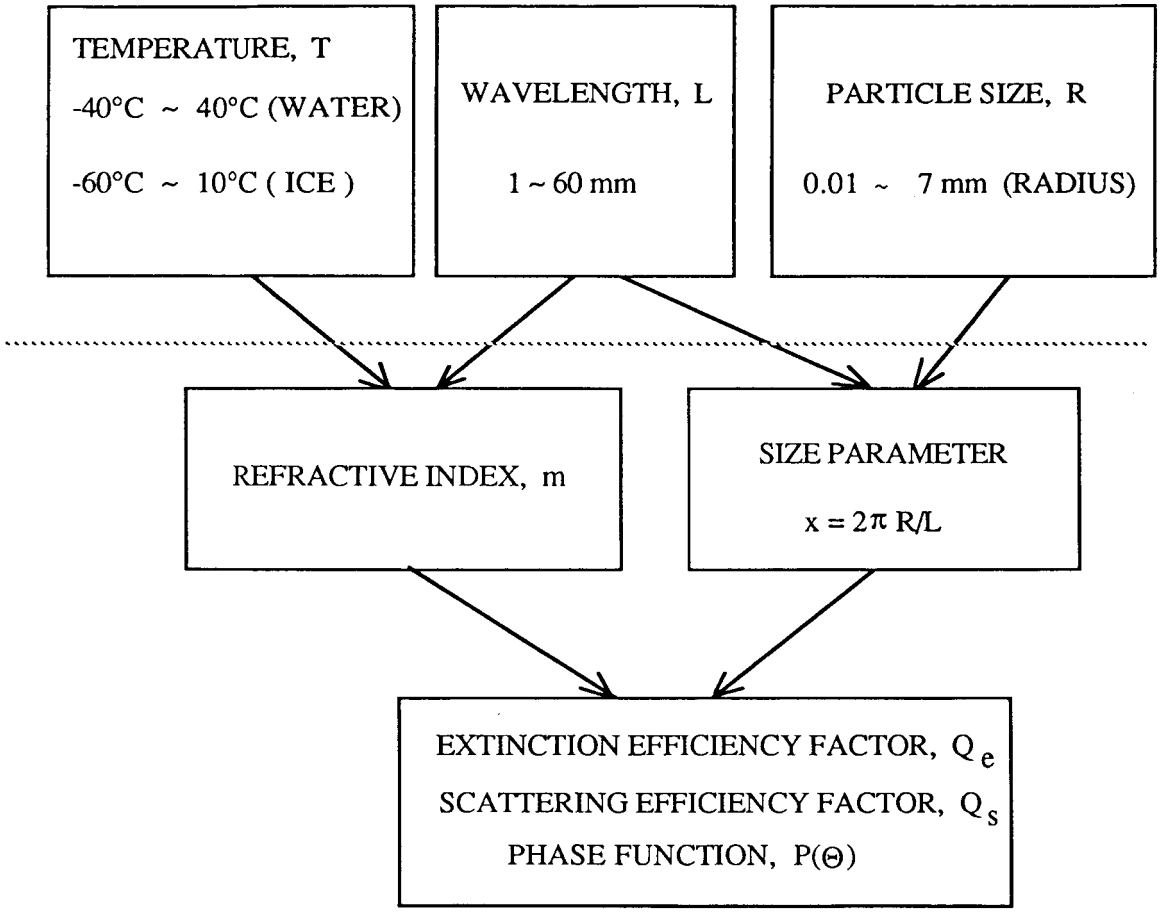

Fig. 2. Schematic flow chart for the Mie calculation.

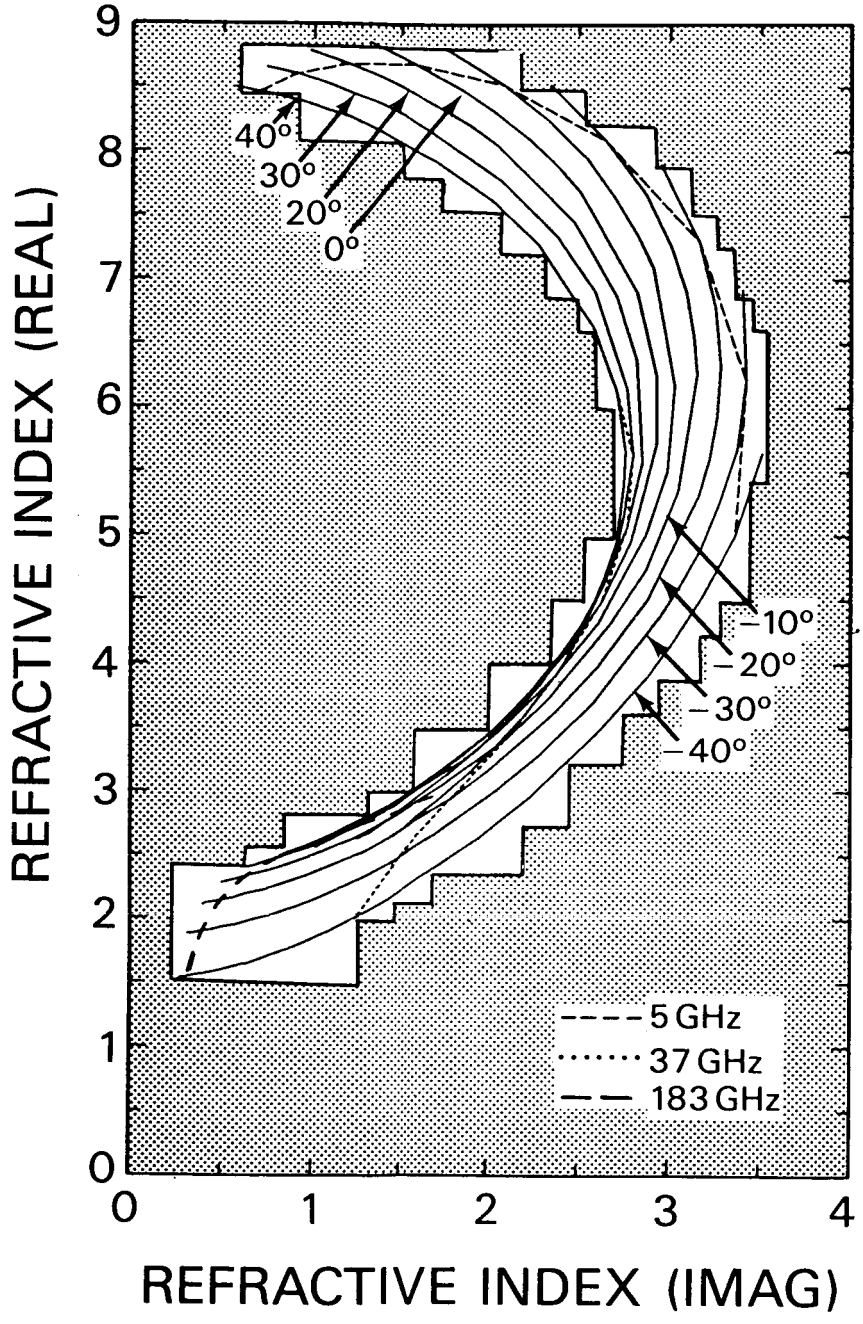

Fig. 3. The complex refractive index, m, as a function of temperature and frequency (Ray, 1972). The values of m in the shaded area is not included in the water tables. Three frequencies are depicted with 5 GHz as lower boundary for the low frequency table, 37 GHz as a differentiation between low and high frequency parts of the water tables, and 183 GHz as higher boundary for the high frequency table.

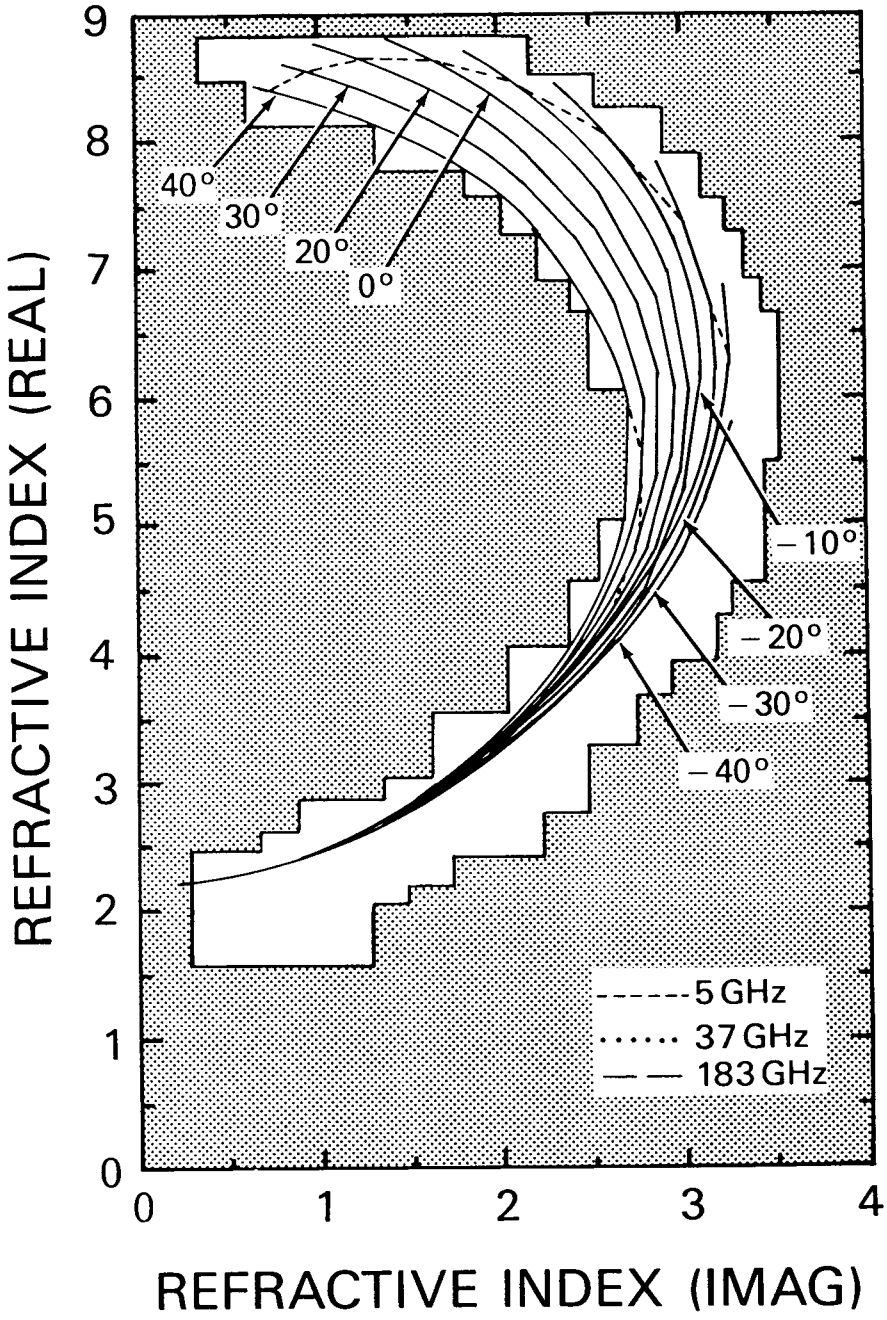

Fig. 4. Same as Fig. 3, except from Lane and Saxton (1952).

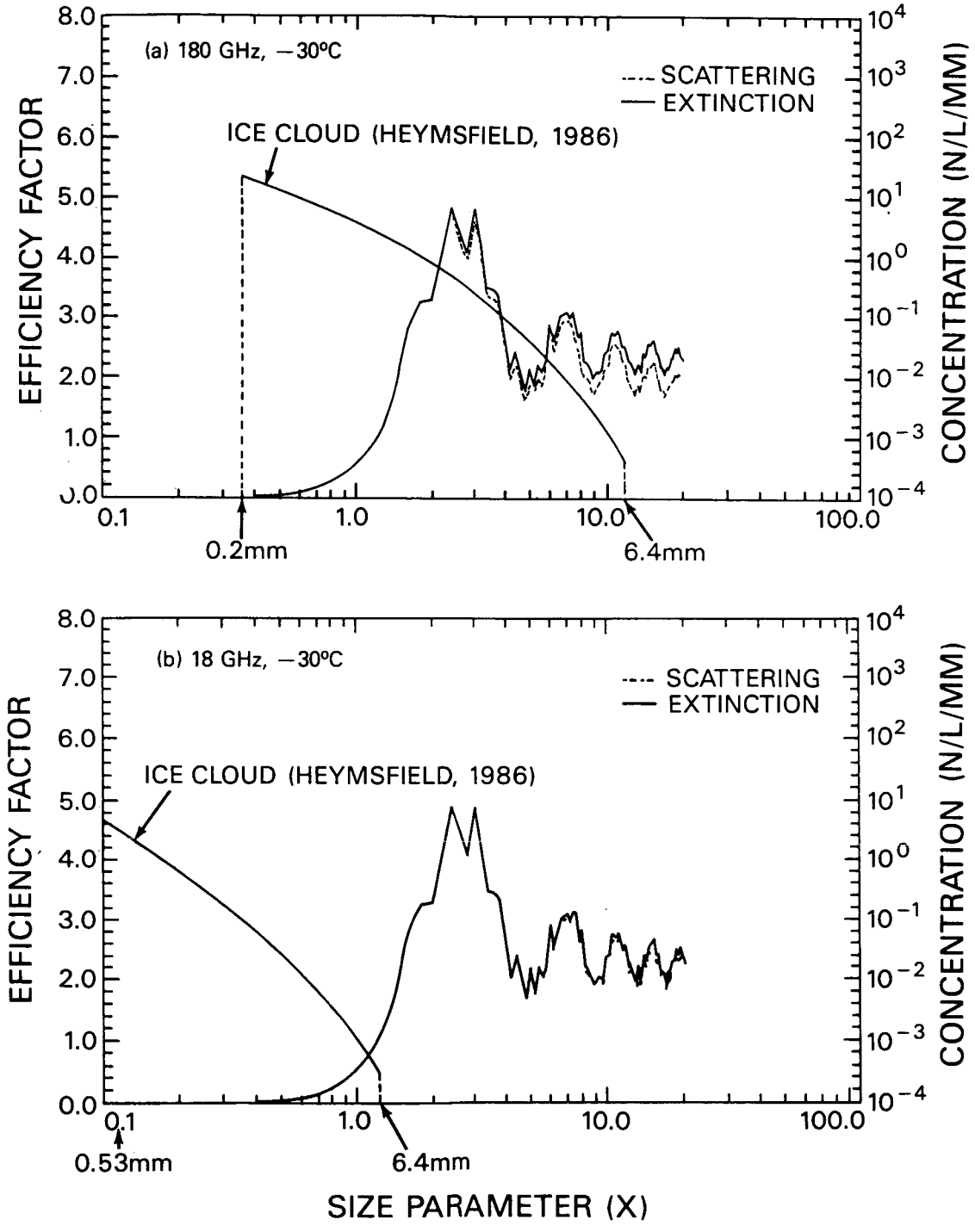

Fig. 5. Mie scattering by ice particles for (a) 180 and (b) 18 GHz. The size distribution, based on aircraft measurements in the anvil region (Heymsfield, 1986), is converted to the scale of size parameter in the diagrams.

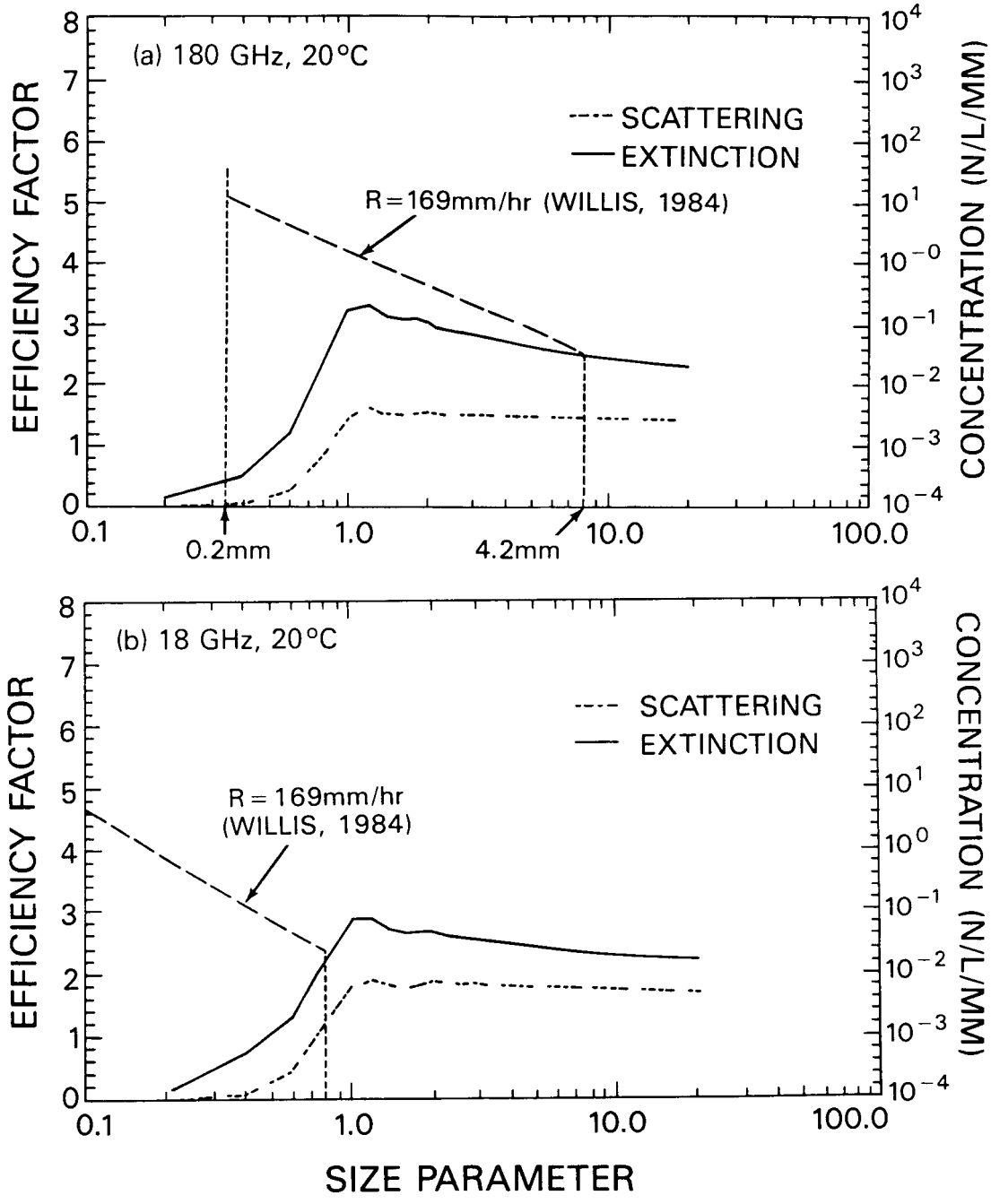

Fig. 6. Same as Fig. 5, except for liquid water droplets. The size distribution is based on the Marshall-Palmer exponential fits for rain rate at 169 mm/hr (Willis, 1984).

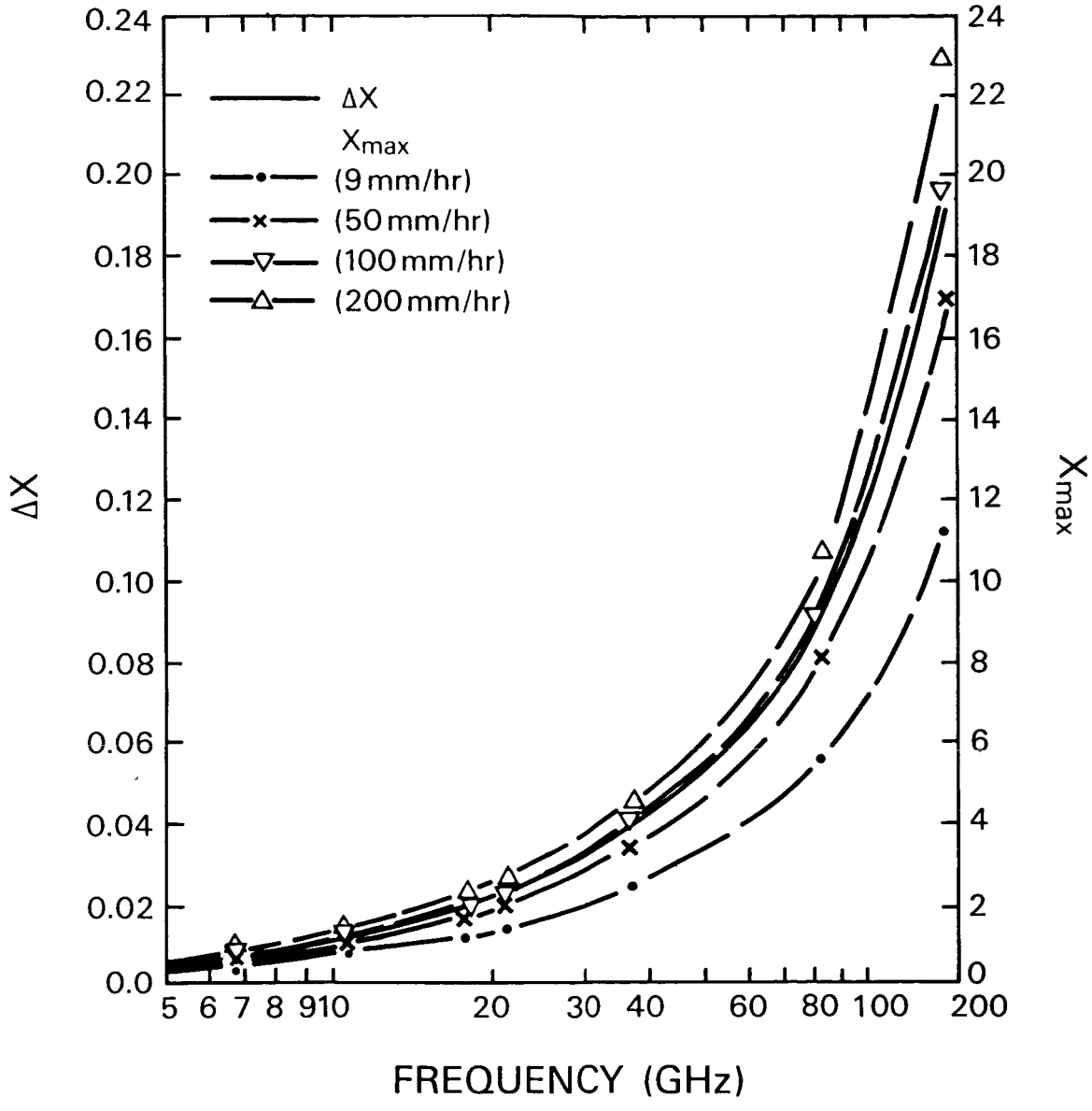

Fig. 7. The resolution of x (Δx) and the maximum value of x (x_{max}) in the Mie tables shown as function of frequency and rain rate.

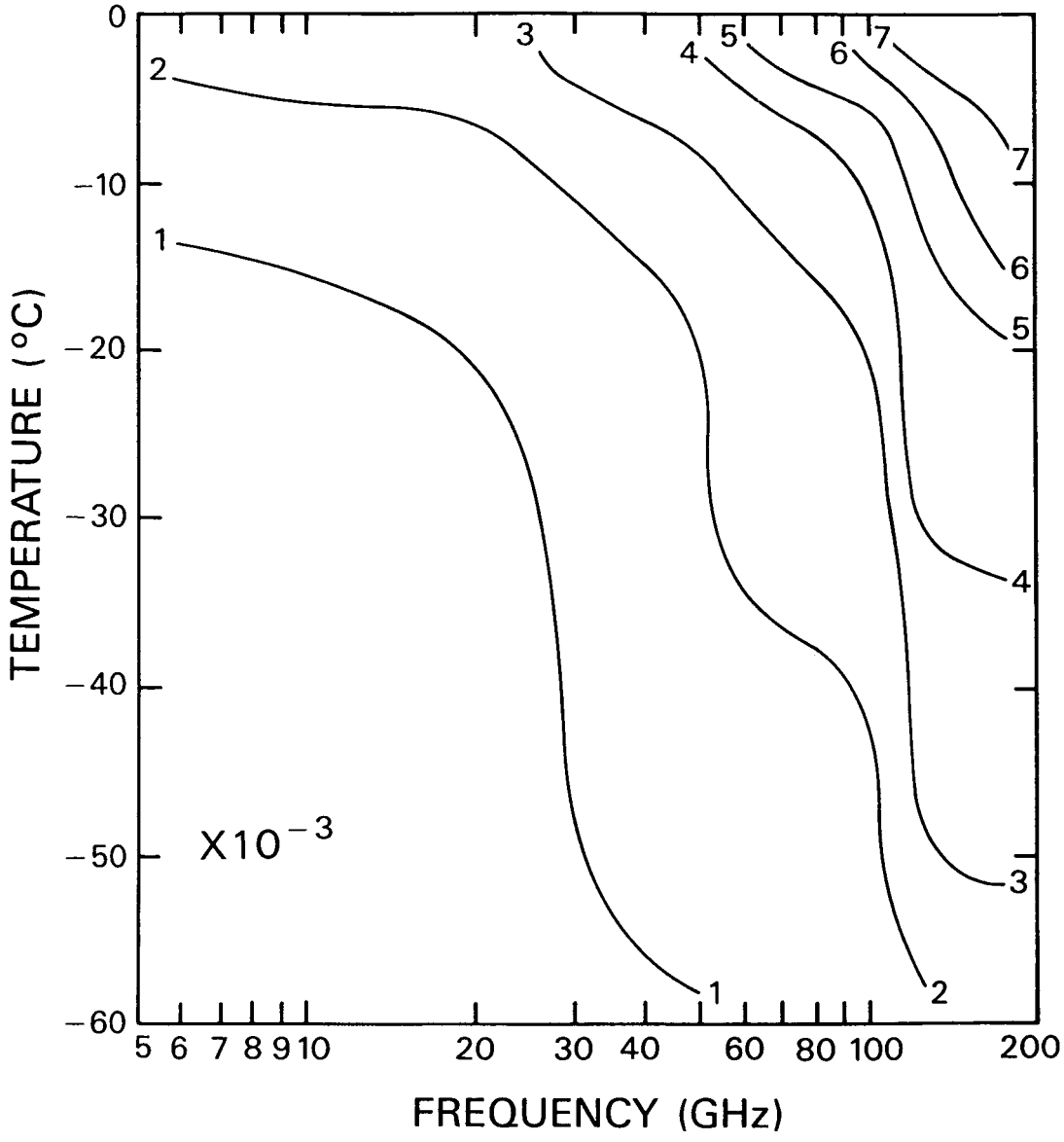

Fig. 8. Imaginary refractive index of ice as a function of temperature and frequency.

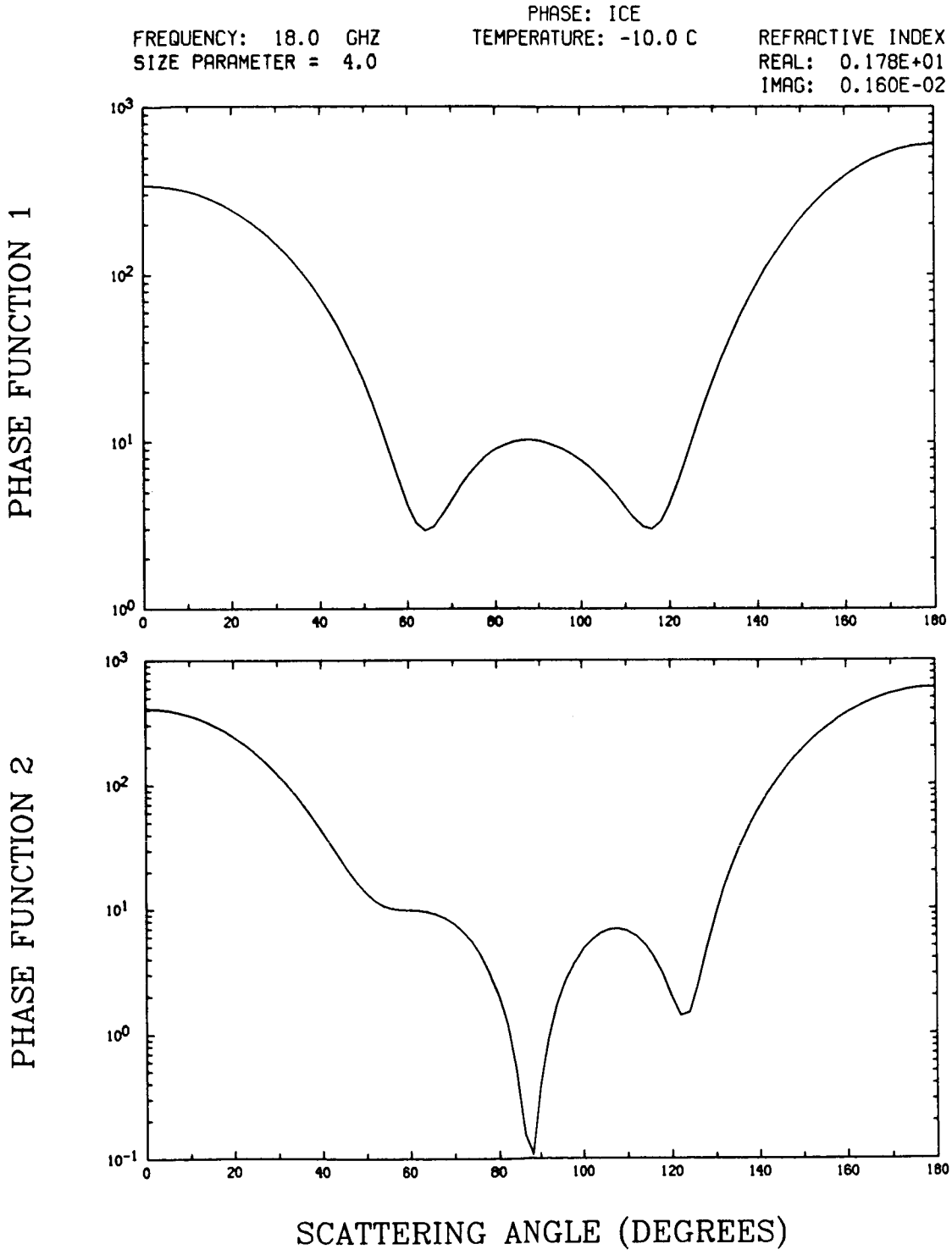

Fig. 9. First and second phase functions of ice for 18 GHz and $x = 4$. The four phase functions are defined in the text.

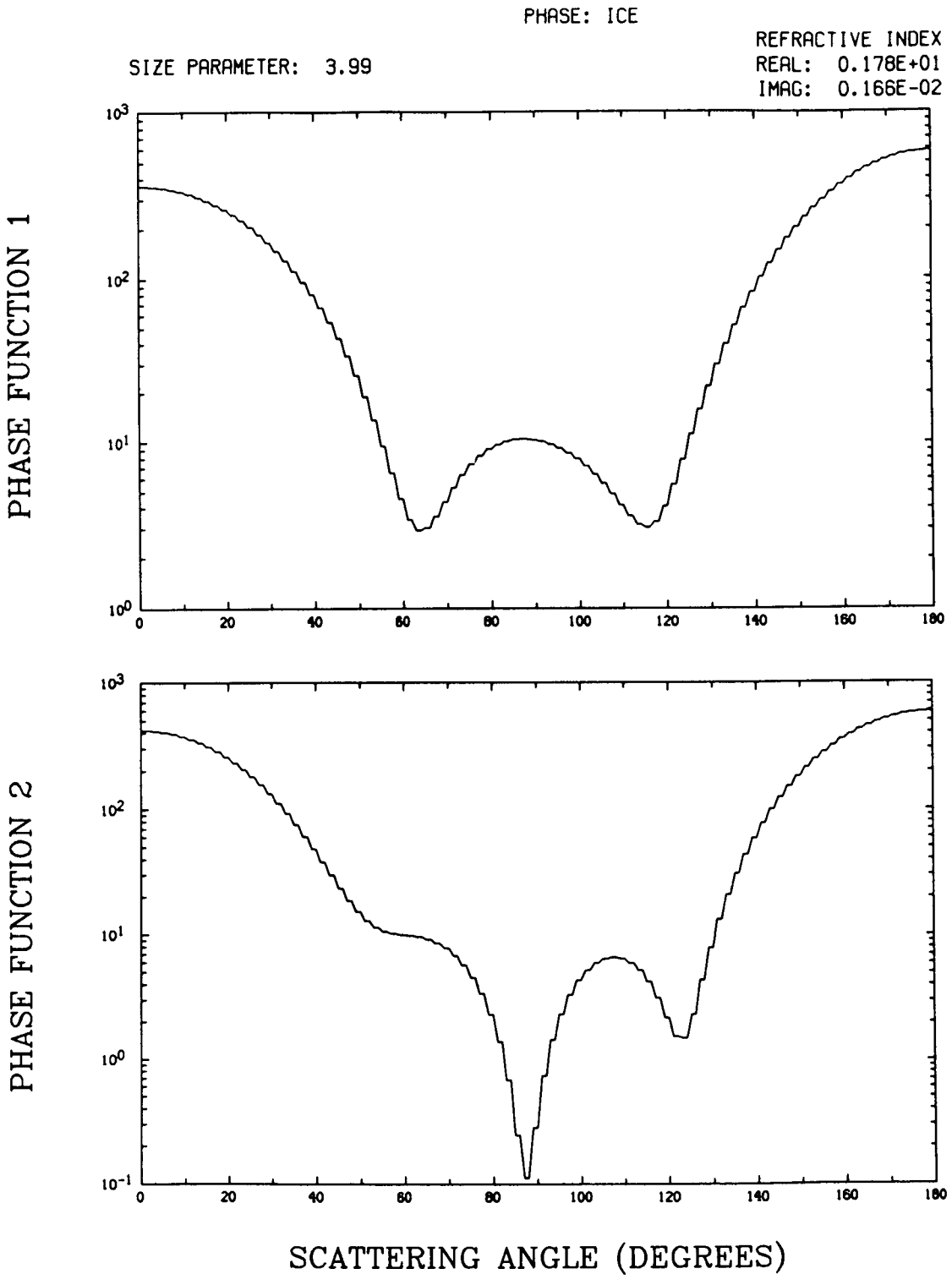

Fig. 10. Averaging phase angles by every 2° for the case of Fig. 9.

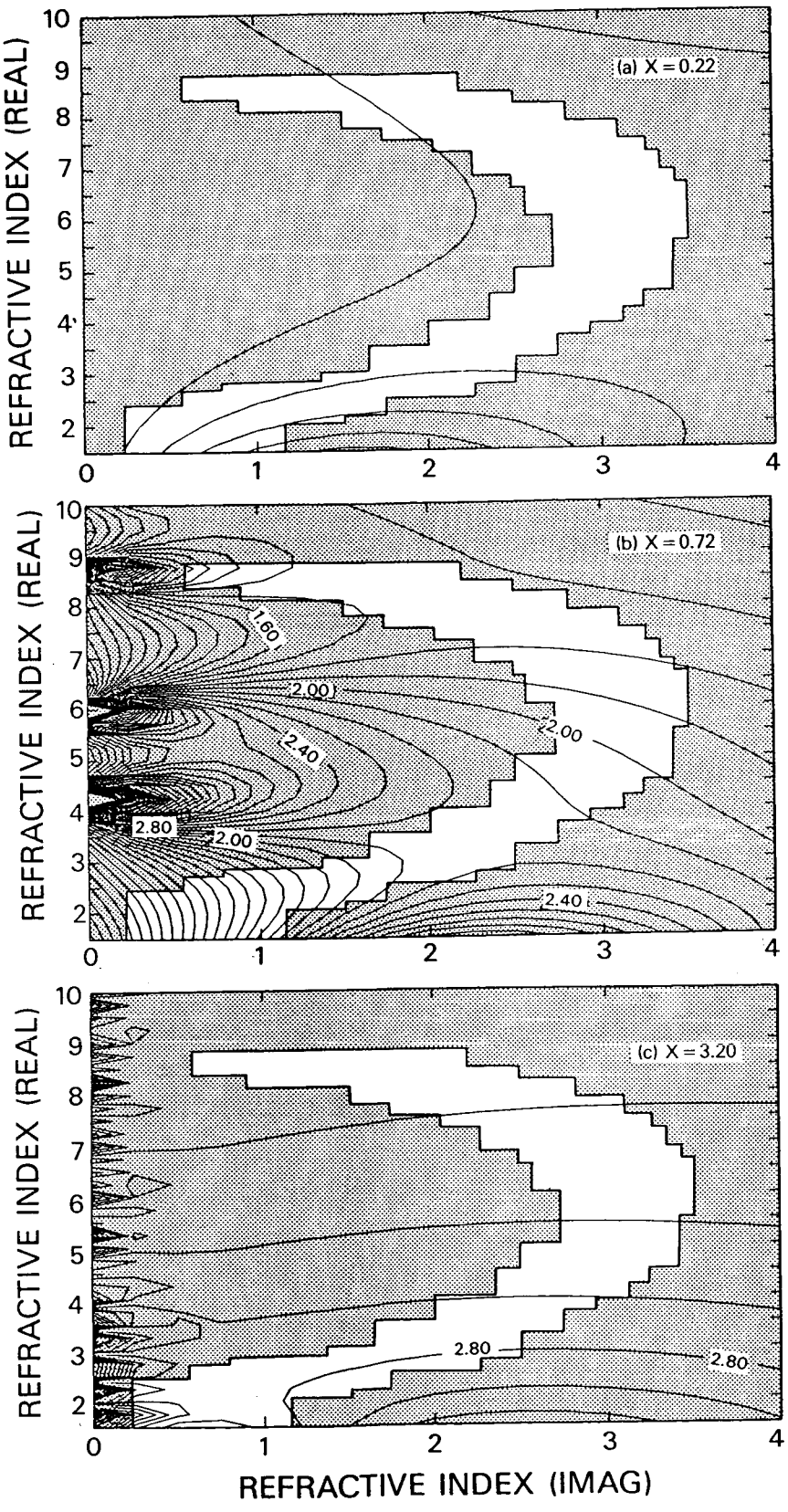

Fig. 11. Extinction efficiency factor of liquid water as a function of the complex refractive index for (a) $x = 0.22$, (b) $x = 0.72$ and (c) $x = 3.20$. The shaded area is equivalent to those in Figs. 3 and 4.

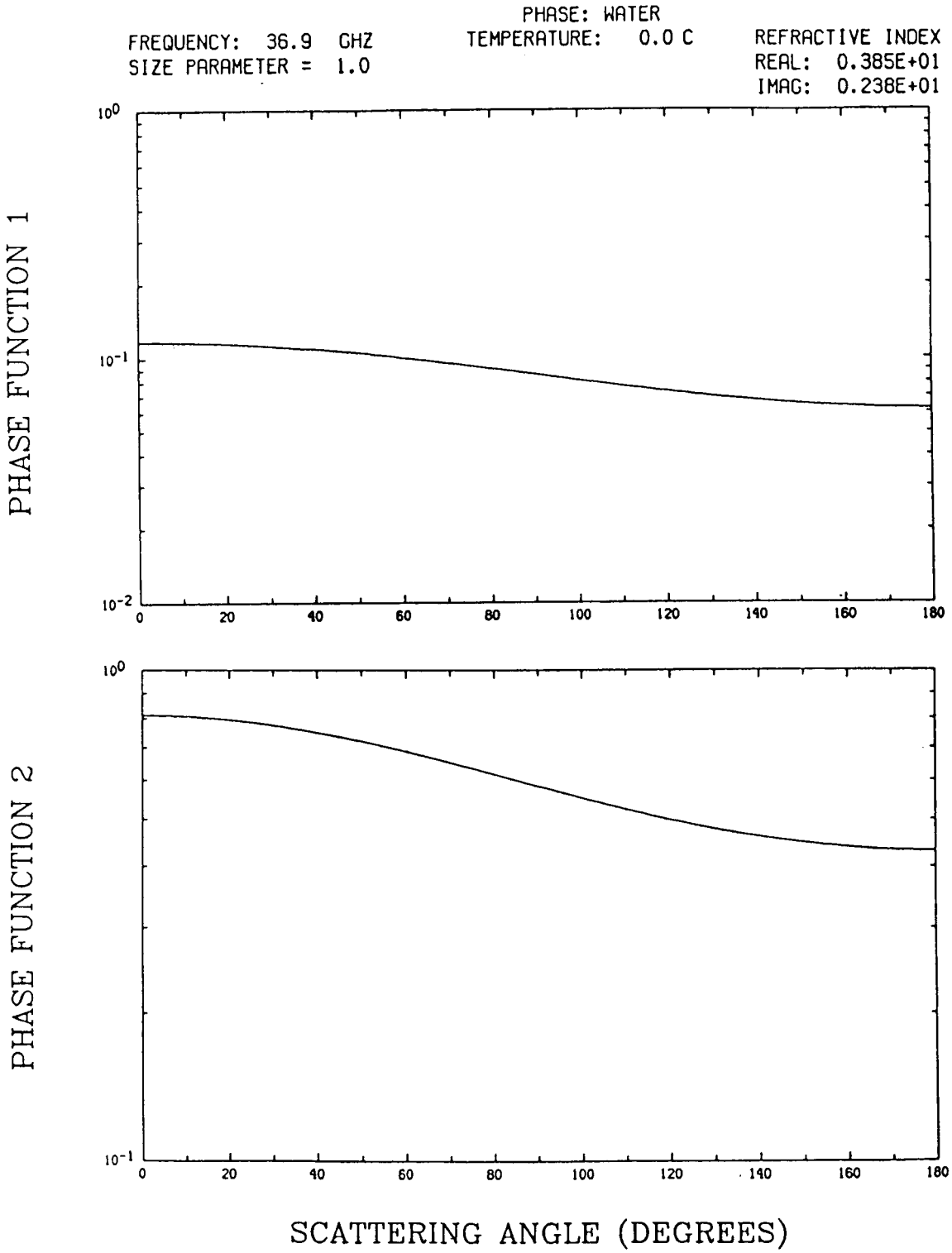

Fig. 12. The four phase functions for liquid water at 37 GHz, 0°C, and $x = 1$.

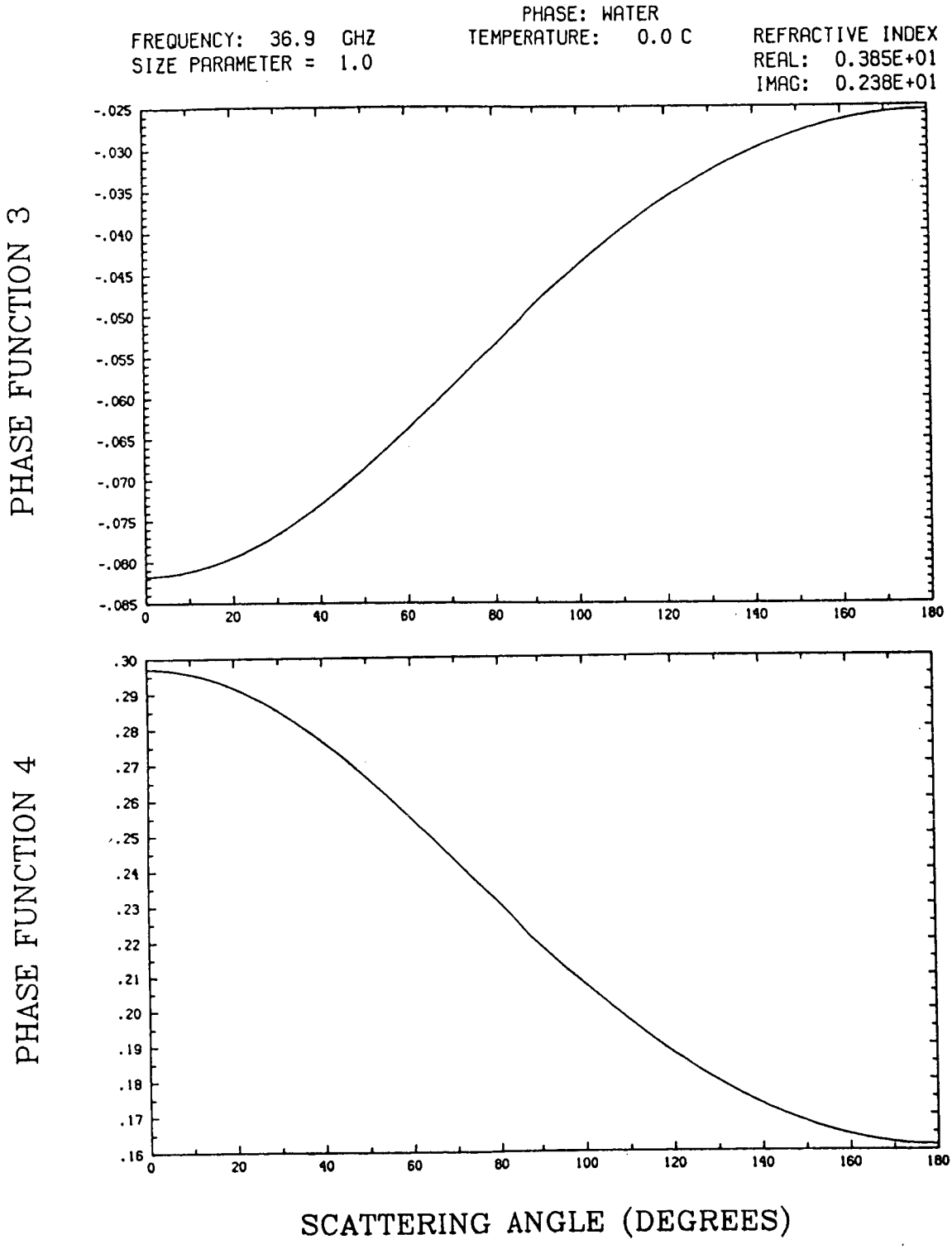

Fig. 12. (Continued)

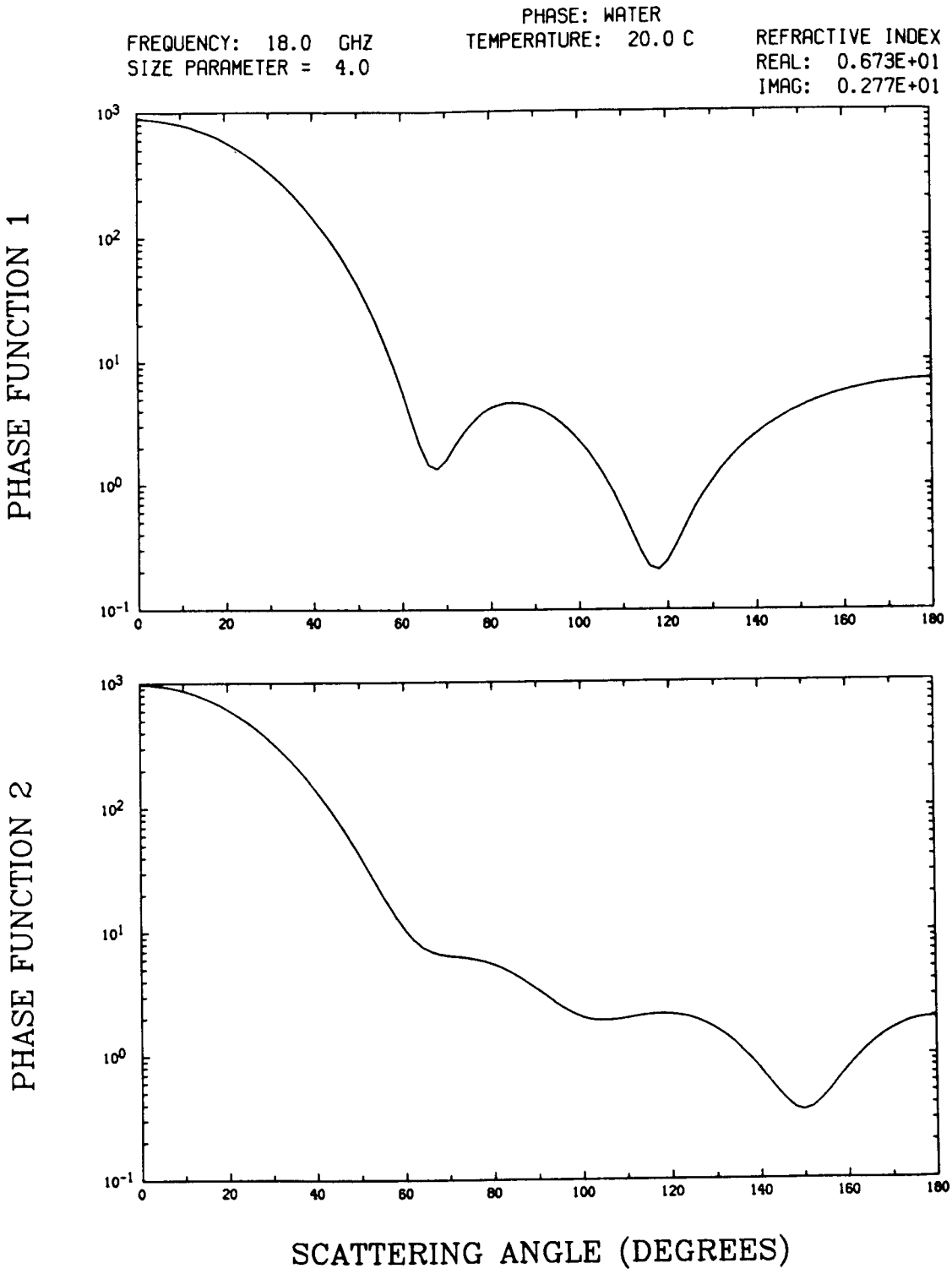

Fig. 13. The first two phase functions for a liquid water at 18 GHz, 20°C, and $x = 4$.

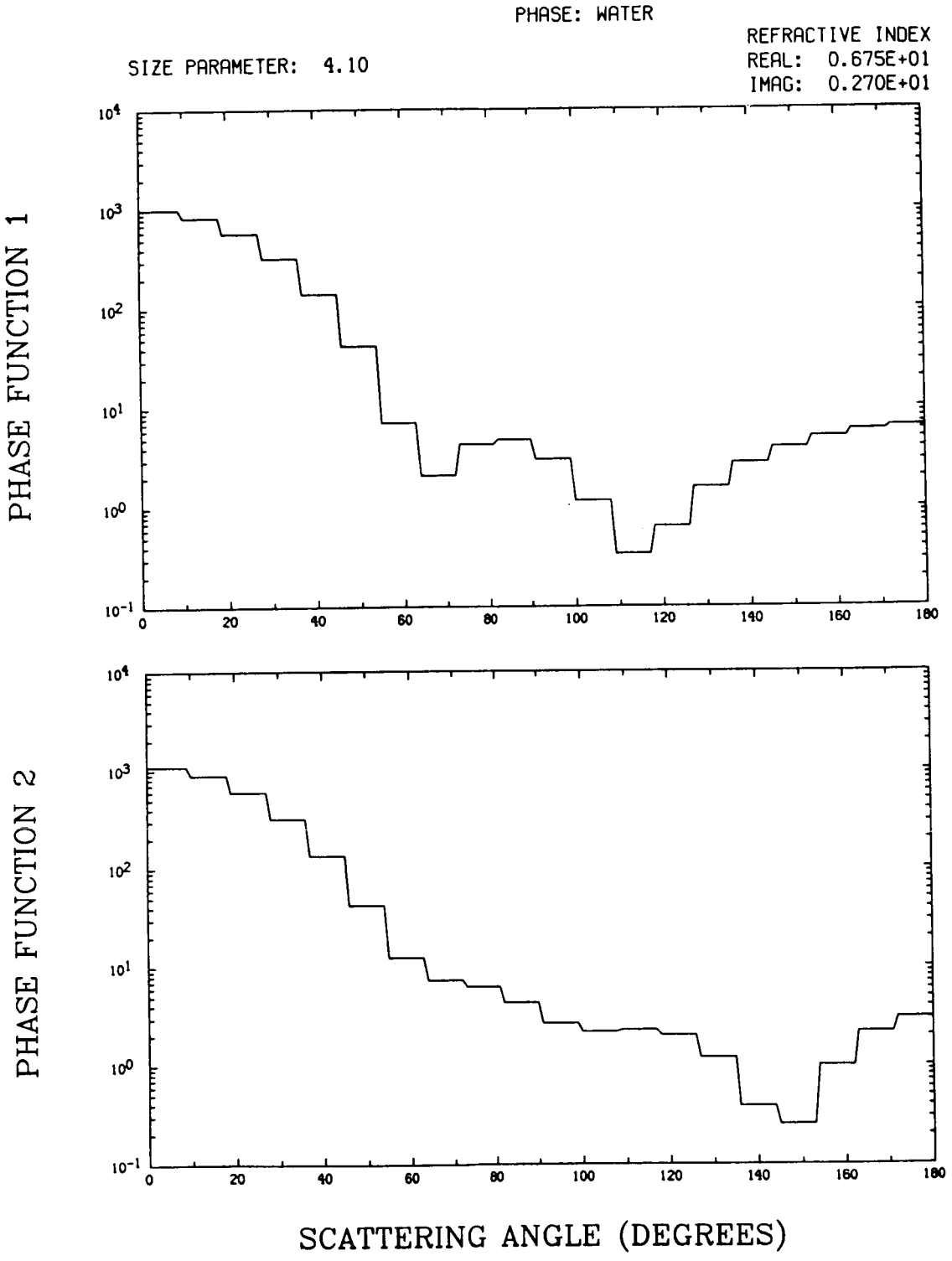

Fig. 14. Averaging phase angles by every 9° for the case of Fig. 13.

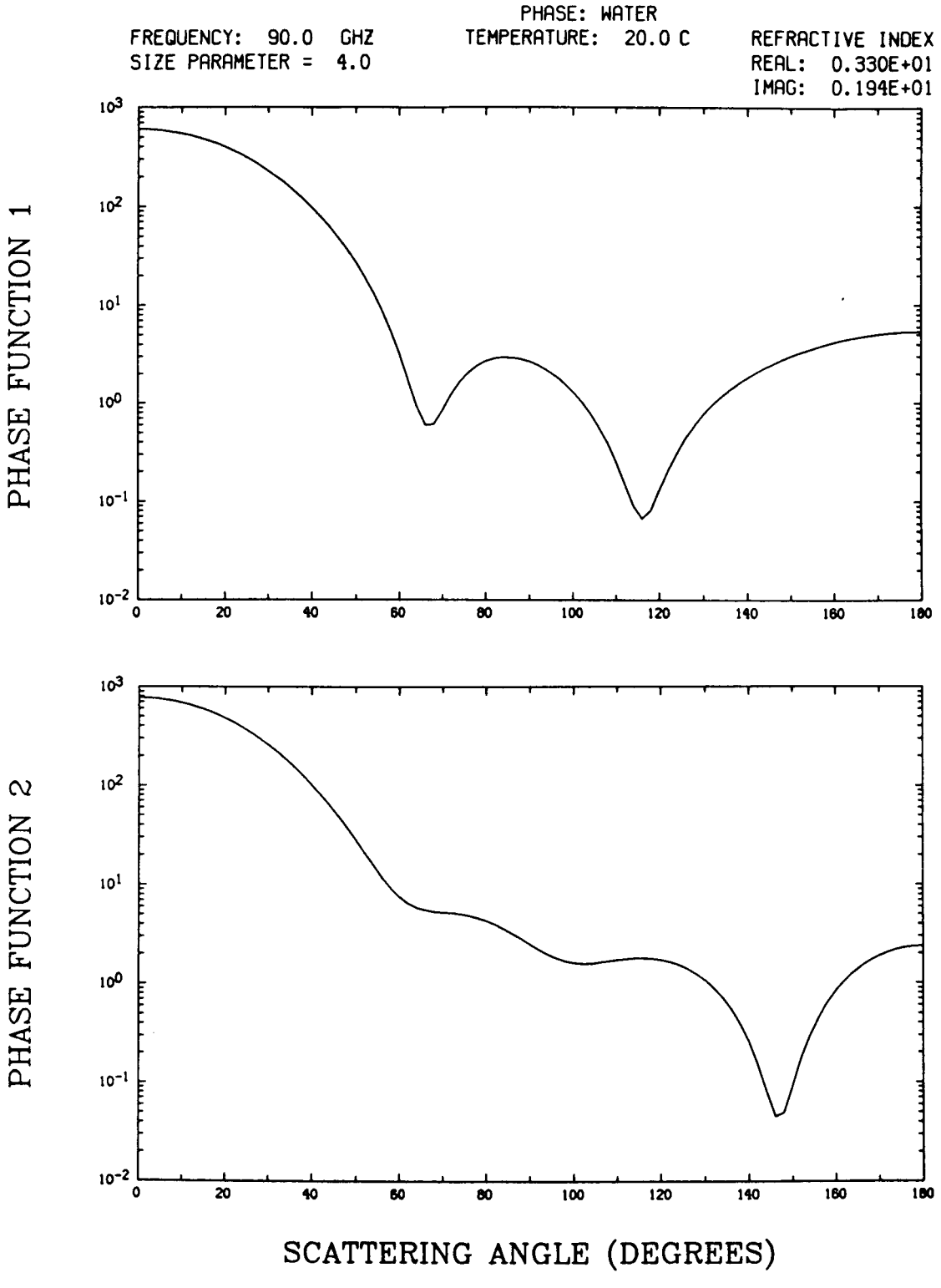

Fig. 15. Same as Fig. 13, except for 90 GHz.

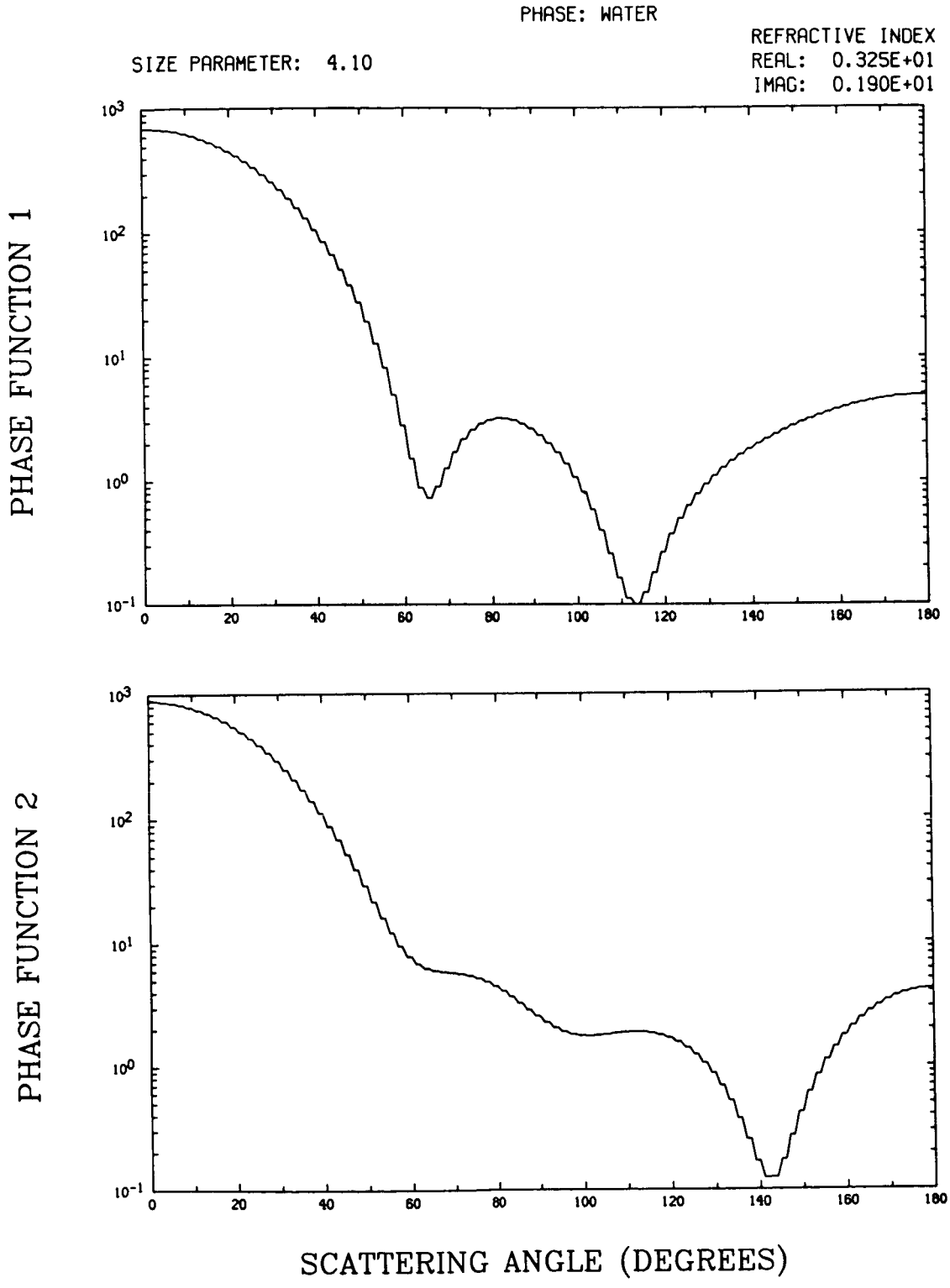

Fig. 16. Averaging phase angles by every 2° for the case of Fig. 15.

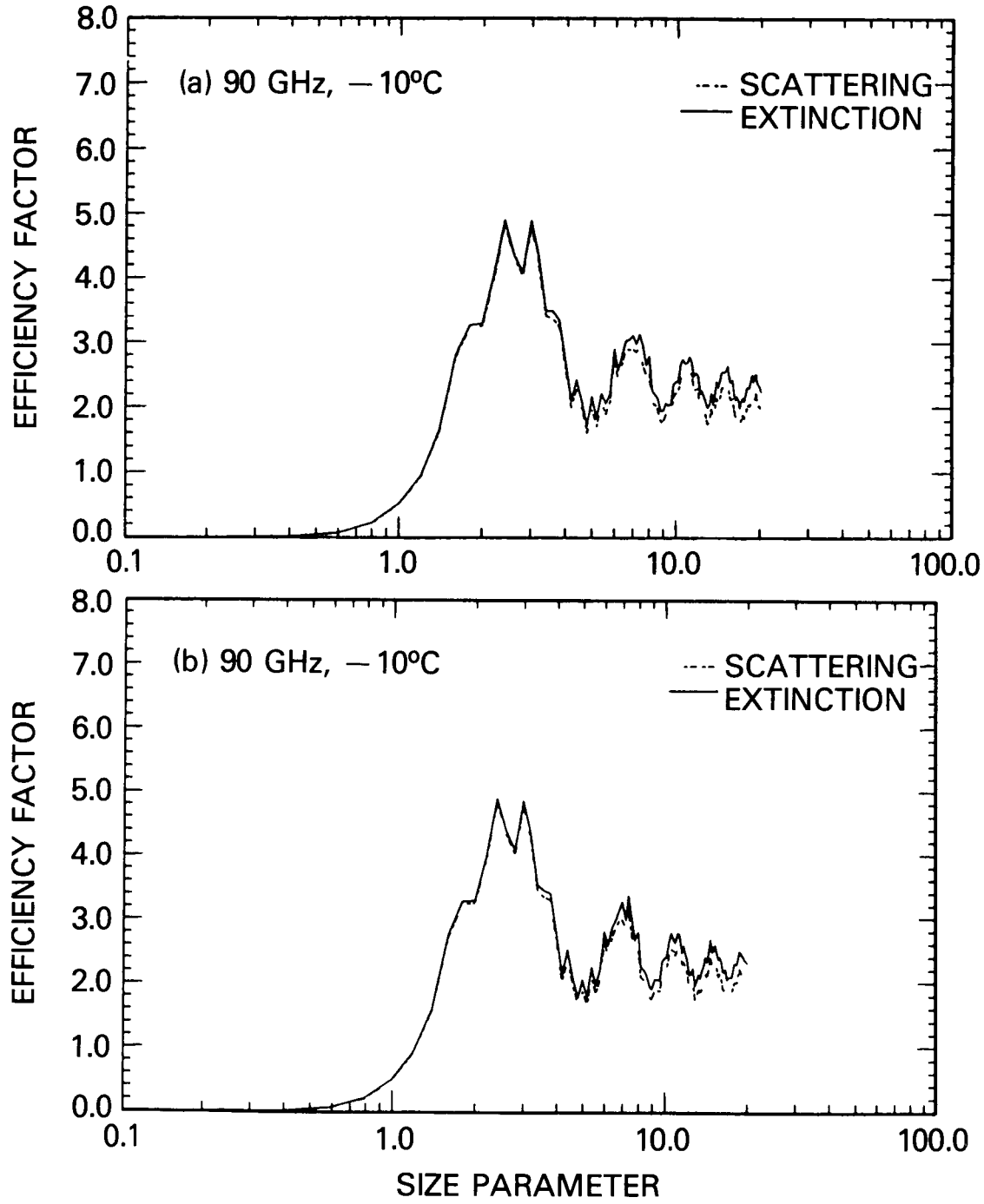

Fig. 17. Comparison of the Mie scattering by ice particles between (a) computation from the Mie codes, and (b) retrieval from the Mie tables. Both diagrams are plotted in resolution of $x = 0.2$.

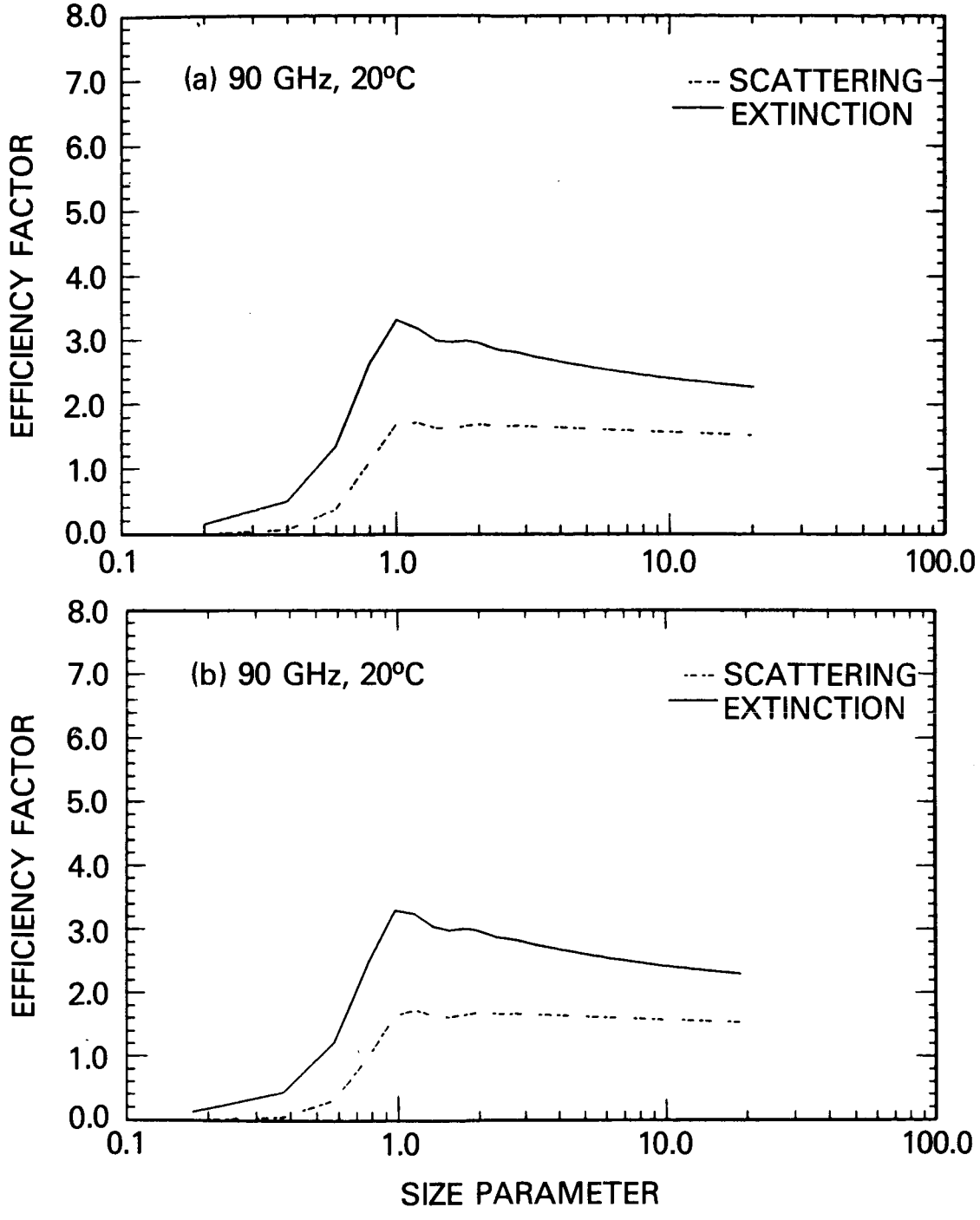

Fig. 18. Same as Fig. 17, except for liquid water droplets.

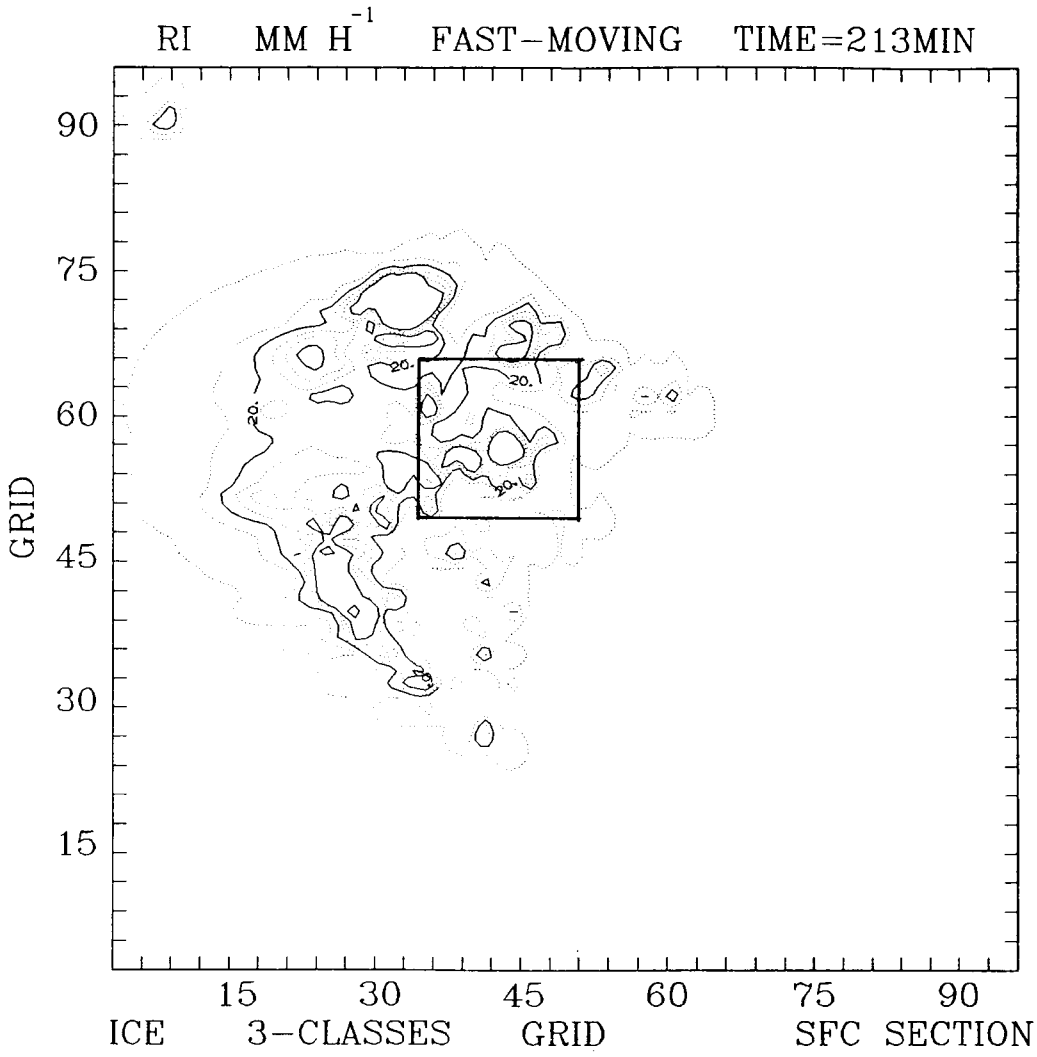

Fig. 19. Results of rain rate calculated from Tao's 3-D cloud model for simulation of GATE fast-moving squall line. The square box is 12X12 grids used for testing the Mie tables.

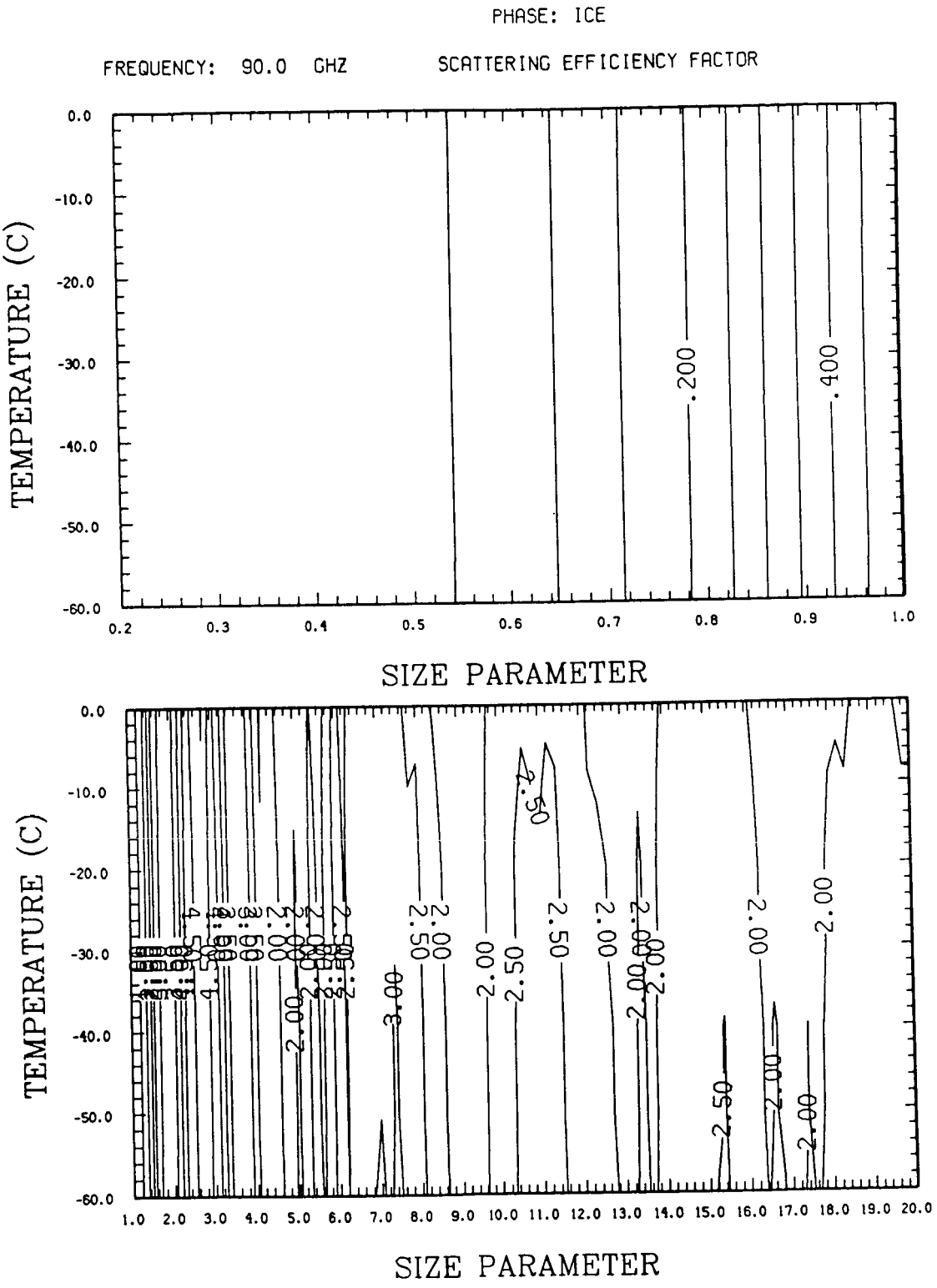

Fig. 20. Scattering efficiency factor of ice as a function of temperatures (plotted in two different ranges of size parameter).

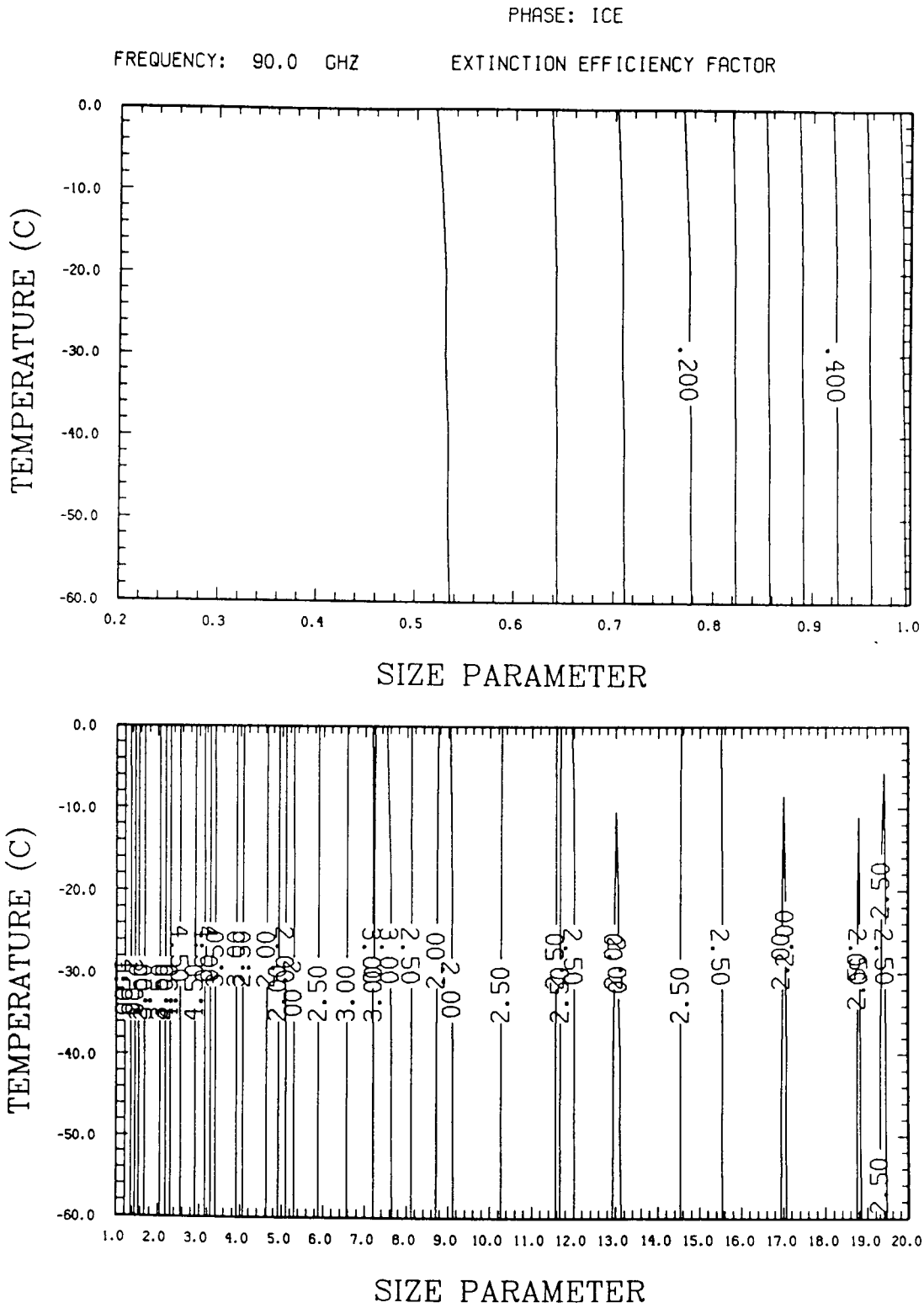

Fig. 21. Same as Fig. 20, except for extinction efficiency factor.

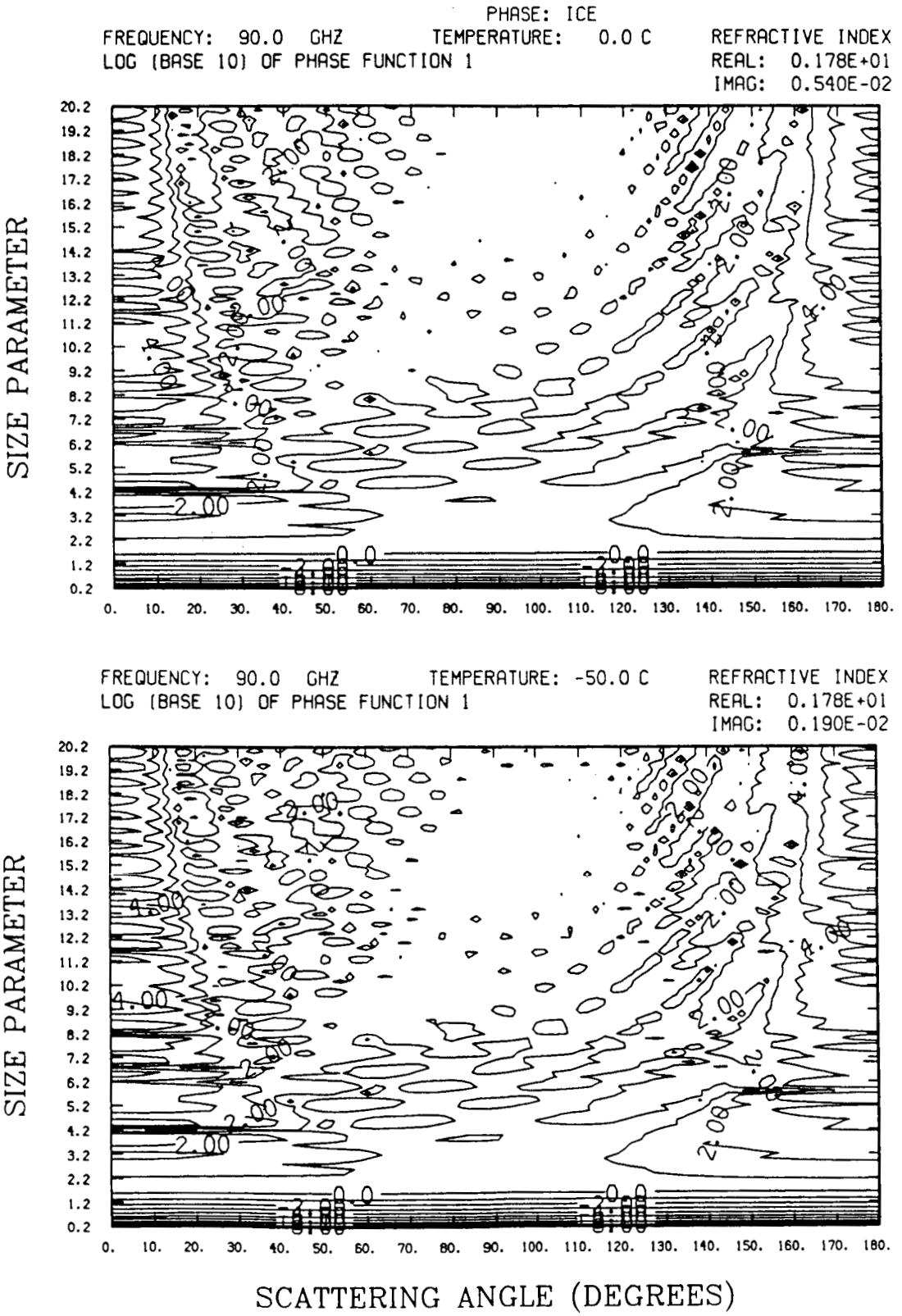

Fig. 22. The first phase function of the Mie scattering by ice particles for 90 GHz at 0°C. The phase function is plotted as a function of scattering angle and size parameter.

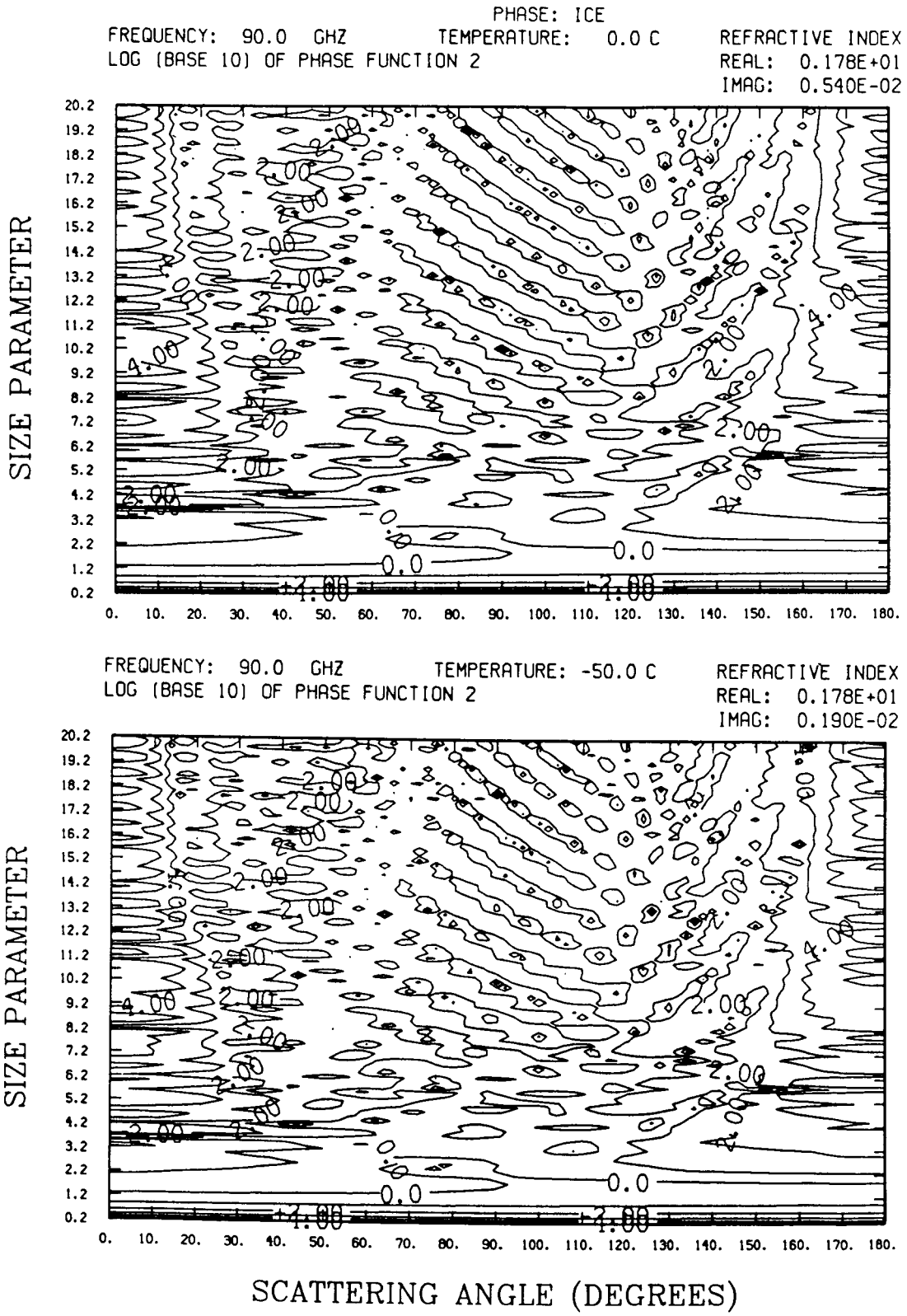

Fig. 23. Same as Fig. 22, except for the second phase function.

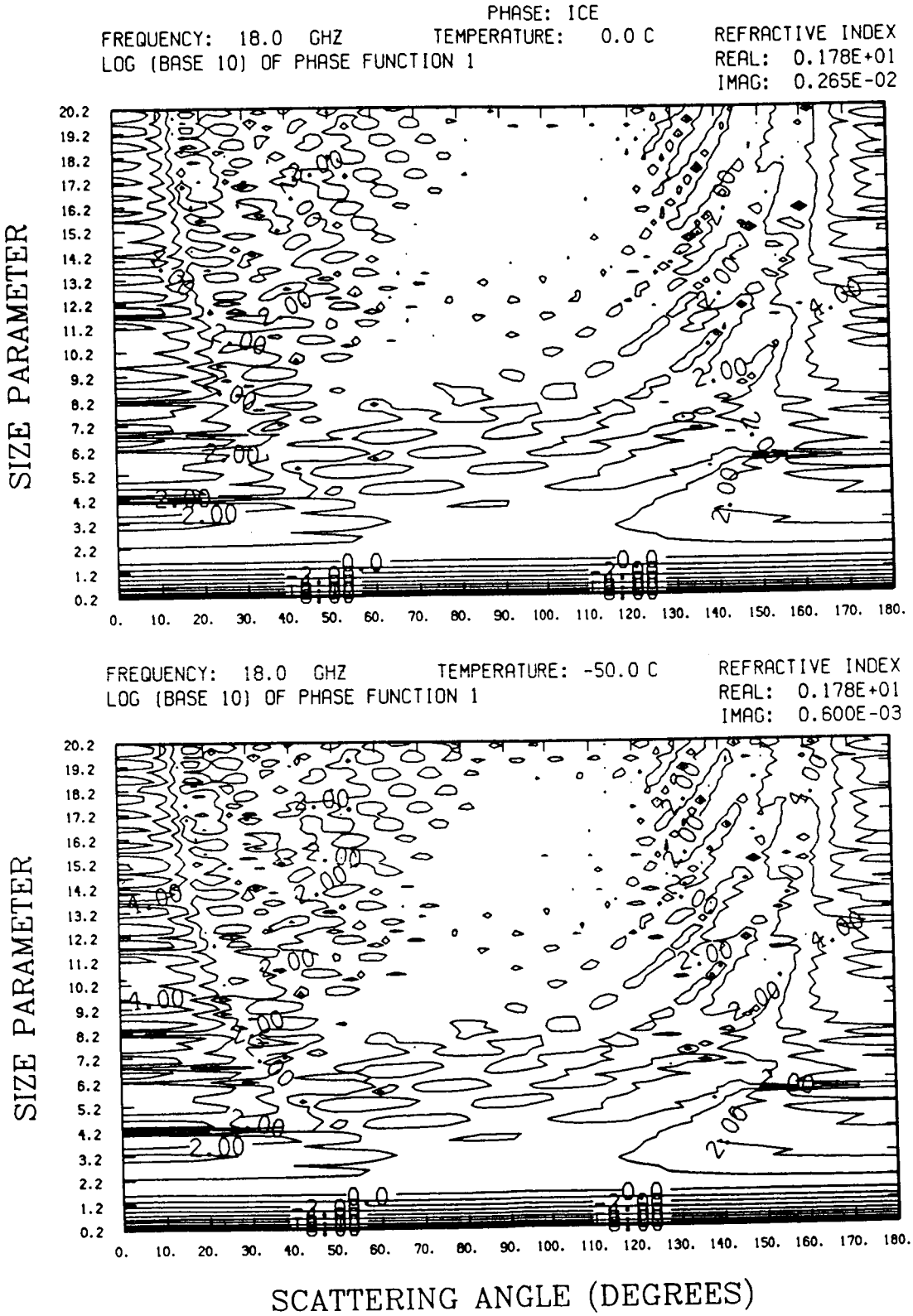

Fig. 24. Same as Fig. 22, except for 18 GHz.

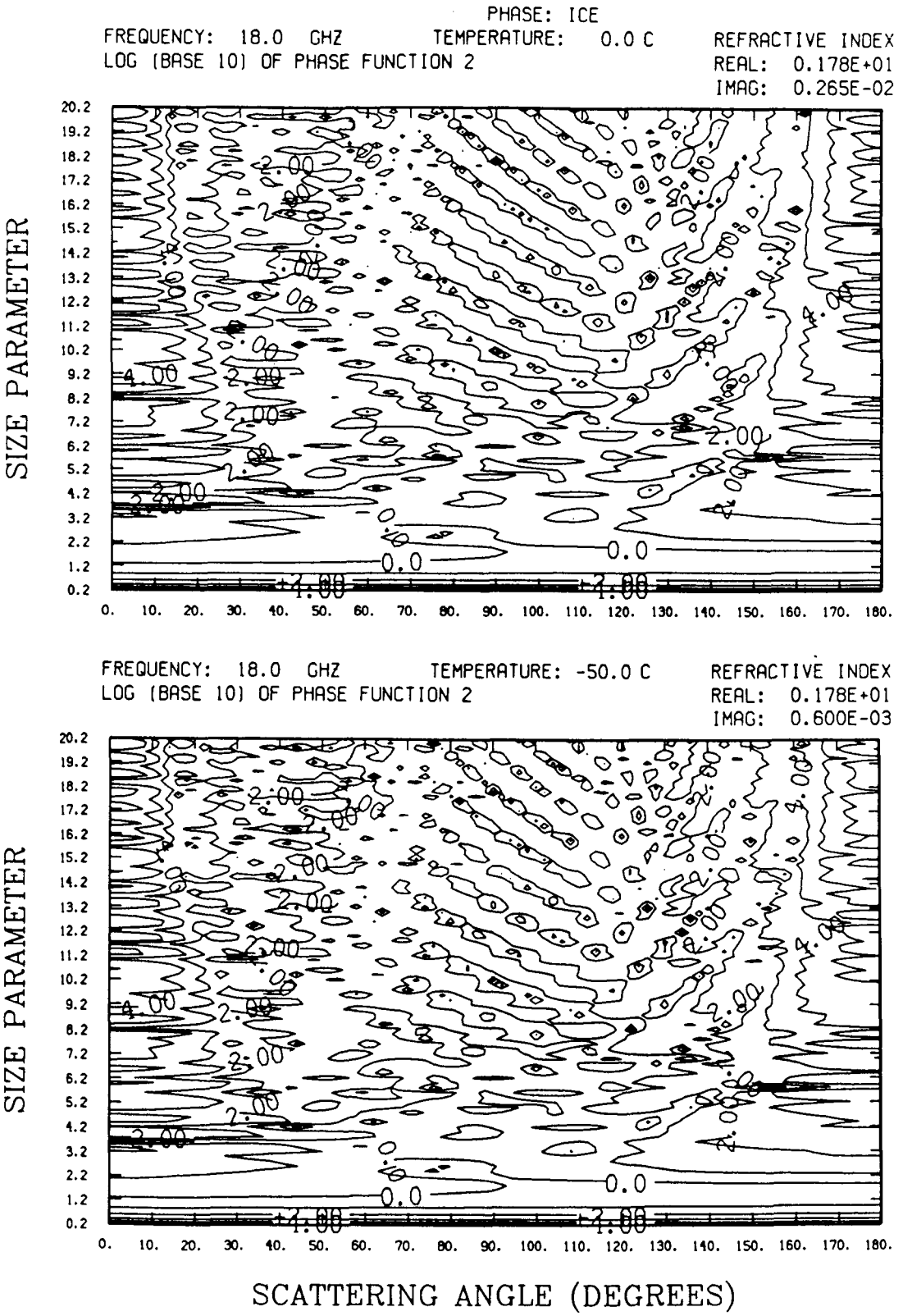

Fig. 25. Same as Fig. 23, except for 18 GHz.

APPENDIX A : ICE TABLE

Table A.1. Resolution and range of imaginary index

No.	Range (X 1.E-3)		Discrete values for averaging (X 1.E-3)
	Lower	Upper	
1	0.4	1.0	0.40, 0.60, 0.70, 0.80, 0.95, 1.00
2	1.0	2.0	1.30, 1.50, 1.60, 1.90, 2.00
3	2.0	3.0	2.30, 2.65, 2.70, 3.00
4	3.0	4.0	3.60, 3.80
5	4.0	5.0	4.60
6	5.0	6.0	5.40, 5.80
7	6.0	7.0	7.40

Table A.2. Size Parameter (x)

Range		dx	x representing	Range		dx	x representing
lower	upper		range	lower	upper		range
1.E-4	1.E-3	1.E-3	5.E-4	0.84	0.86	0.02	0.85
1.E-3	8.E-3	7.E-3	5.E-3	0.86	0.88	0.02	0.87
8.E-3	1.5E-2	7.E-3	0.012	0.88	0.90	0.02	0.89
0.015	0.022	0.007	0.019	0.90	0.92	0.02	0.91
0.022	0.029	0.007	0.026	0.92	0.94	0.02	0.93
0.029	0.036	0.007	0.033	0.94	0.96	0.02	0.95
0.036	0.43	0.007	0.040	0.96	0.98	0.02	0.97
0.043	0.05	0.007	0.047	0.98	1.00	0.02	0.99
0.050	0.06	0.01	0.055	1.00	1.02	0.02	1.01
0.060	0.07	0.01	0.065	1.02	1.04	0.02	1.03
0.070	0.08	0.01	0.075	1.04	1.06	0.02	1.05
0.080	0.09	0.01	0.085	1.06	1.08	0.02	1.07
0.090	0.10	0.01	0.095	1.08	1.10	0.02	1.09
0.10	0.12	0.02	0.11	1.10	1.12	0.02	1.11
0.12	0.14	0.02	0.13	1.12	1.14	0.02	1.13
0.14	0.16	0.02	0.15	1.14	1.16	0.02	1.15
0.16	0.18	0.02	0.17	1.16	1.18	0.02	1.17
0.18	0.20	0.02	0.19	1.18	1.20	0.02	1.19
0.20	0.22	0.02	0.21	1.20	1.22	0.02	1.21
0.22	0.24	0.02	0.23	1.22	1.24	0.02	1.23
0.24	0.26	0.02	0.25	1.24	1.26	0.02	1.25
0.26	0.28	0.02	0.27	1.26	1.28	0.02	1.27
0.28	0.30	0.02	0.29	1.28	1.30	0.02	1.29
0.30	0.32	0.02	0.31	1.30	1.32	0.02	1.31
0.32	0.34	0.02	0.33	1.32	1.34	0.02	1.33
0.34	0.36	0.02	0.35	1.34	1.36	0.02	1.35
0.36	0.38	0.02	0.37	1.36	1.38	0.02	1.37
0.38	0.40	0.02	0.39	1.38	1.40	0.02	1.39
0.40	0.42	0.02	0.41	1.40	1.42	0.02	1.41
0.42	0.44	0.02	0.43	1.42	1.44	0.02	1.43
0.44	0.46	0.02	0.45	1.44	1.46	0.02	1.45
0.46	0.48	0.02	0.47	1.46	1.48	0.02	1.47
0.48	0.50	0.02	0.49	1.48	1.50	0.02	1.49
0.50	0.52	0.02	0.51	1.50	1.52	0.02	1.51
0.52	0.54	0.02	0.53	1.52	1.54	0.02	1.53
0.54	0.56	0.02	0.55	1.54	1.56	0.02	1.55
0.56	0.58	0.02	0.57	1.56	1.58	0.02	1.57
0.58	0.60	0.02	0.59	1.58	1.60	0.02	1.59
0.60	0.62	0.02	0.61	1.60	1.62	0.02	1.61
0.62	0.64	0.02	0.63	1.62	1.64	0.02	1.63
0.64	0.66	0.02	0.65	1.64	1.66	0.02	1.65
0.66	0.68	0.02	0.67	1.66	1.68	0.02	1.67
0.68	0.70	0.02	0.69	1.68	1.70	0.02	1.69
0.70	0.72	0.02	0.71	1.70	1.72	0.02	1.71
0.72	0.74	0.02	0.73	1.72	1.74	0.02	1.73
0.74	0.76	0.02	0.75	1.74	1.76	0.02	1.75
0.76	0.78	0.02	0.77	1.76	1.78	0.02	1.77
0.78	0.80	0.02	0.79	1.78	1.80	0.02	1.79
0.80	0.82	0.02	0.81	1.80	1.82	0.02	1.81
0.82	0.84	0.02	0.83	1.82	1.84	0.02	1.83

Table A.2. Size Parameter (x) (continued)

Range		dx	x representing	Range		dx	x representing
lower	upper		range	lower	upper		range
1.84	1.86	0.02	1.85	2.84	2.84	0.02	2.85
1.86	1.88	0.02	1.87	2.86	2.86	0.02	2.87
1.88	1.90	0.02	1.89	2.88	2.90	0.02	2.89
1.90	1.92	0.02	1.91	2.90	2.92	0.02	2.91
1.92	1.94	0.02	1.93	2.92	2.94	0.02	2.93
1.94	1.96	0.02	1.95	2.94	2.96	0.02	2.95
1.96	1.98	0.02	1.97	2.96	2.98	0.02	2.97
1.98	2.00	0.02	1.99	2.98	3.00	0.02	2.99
2.00	2.02	0.02	2.01	3.00	3.02	0.02	3.01
2.02	2.04	0.02	2.03	3.02	3.04	0.02	3.03
2.04	2.06	0.02	2.05	3.04	3.06	0.02	3.05
2.06	2.08	0.02	2.07	3.06	3.08	0.02	3.07
2.08	2.10	0.02	2.09	3.08	3.10	0.02	3.09
2.10	2.12	0.02	2.11	3.10	3.12	0.02	3.11
2.12	2.14	0.02	2.13	3.12	3.14	0.02	3.13
2.14	2.16	0.02	2.15	3.14	3.16	0.02	3.15
2.16	2.18	0.02	2.17	3.16	3.18	0.02	3.17
2.18	2.20	0.02	2.19	3.18	3.20	0.02	3.19
2.20	2.22	0.02	2.21	3.20	3.22	0.02	3.21
2.22	2.24	0.02	2.23	3.22	3.24	0.02	3.23
2.24	2.26	0.02	2.25	3.24	3.26	0.02	3.25
2.26	2.28	0.02	2.27	3.26	3.28	0.02	3.27
2.28	2.30	0.02	2.29	3.28	3.30	0.02	3.29
2.30	2.32	0.02	2.31	3.30	3.32	0.02	3.31
2.32	2.34	0.02	2.33	3.32	3.34	0.02	3.33
2.34	2.36	0.02	2.35	3.34	3.36	0.02	3.35
2.36	2.38	0.02	2.37	3.36	3.38	0.02	3.37
2.38	2.40	0.02	2.39	3.38	3.40	0.02	3.39
2.40	2.42	0.02	2.41	3.40	3.42	0.02	3.41
2.42	2.44	0.02	2.43	3.42	3.44	0.02	3.43
2.44	2.46	0.02	2.45	3.44	3.46	0.02	3.45
2.46	2.48	0.02	2.47	3.46	3.48	0.02	3.47
2.48	2.50	0.02	2.49	3.48	3.50	0.02	3.49
2.50	2.52	0.02	2.51	3.50	3.52	0.02	3.51
2.52	2.54	0.02	2.53	3.52	3.54	0.02	3.53
2.54	2.56	0.02	2.55	3.54	3.56	0.02	3.55
2.56	2.58	0.02	2.57	3.56	3.58	0.02	3.57
2.58	2.60	0.02	2.59	3.58	3.60	0.02	3.59
2.60	2.60	0.02	2.61	3.60	3.62	0.02	3.61
2.62	2.62	0.02	2.63	3.62	3.64	0.02	3.63
2.64	2.64	0.02	2.65	3.64	3.66	0.02	3.65
2.66	2.66	0.02	2.67	3.66	3.68	0.02	3.67
2.68	2.68	0.02	2.69	3.68	3.70	0.02	3.69
2.70	2.70	0.02	2.71	3.70	3.72	0.02	3.71
2.72	2.72	0.02	2.73	3.72	3.74	0.02	3.73
2.74	2.74	0.02	2.75	3.74	3.76	0.02	3.75
2.76	2.76	0.02	2.77	3.76	3.78	0.02	3.77
2.78	2.78	0.02	2.79	3.78	3.80	0.02	3.79
2.80	2.80	0.02	2.81	3.80	3.82	0.02	3.81
2.82	2.82	0.02	2.83	3.82	3.84	0.02	3.83

Table A.2. Size Parameter (x) (continued)

Range		dx	x representing	Range		dx	x representing
lower	upper		range	lower	upper		range
3.84	3.86	0.02	3.85	5.68	5.72	0.04	5.70
3.86	3.88	0.02	3.87	5.72	5.76	0.04	5.74
3.88	3.90	0.02	3.89	5.76	5.80	0.04	5.78
3.90	3.92	0.02	3.91	5.80	5.84	0.04	5.82
3.92	3.94	0.02	3.93	5.84	5.88	0.04	5.86
3.94	3.96	0.02	3.95	5.88	5.92	0.04	5.90
3.96	3.98	0.02	3.97	5.92	5.96	0.04	5.94
3.98	4.00	0.04	3.99	5.96	6.00	0.04	5.98
4.00	4.04	0.04	4.02	6.00	6.04	0.04	6.02
4.04	4.08	0.04	4.06	6.04	6.08	0.04	6.06
4.08	4.12	0.04	4.10	6.08	6.12	0.04	6.10
4.12	4.16	0.04	4.14	6.12	6.16	0.04	6.14
4.16	4.20	0.04	4.18	6.16	6.20	0.04	6.18
4.20	4.24	0.04	4.22	6.20	6.24	0.04	6.22
4.24	4.28	0.04	4.26	6.24	6.28	0.04	6.26
4.28	4.32	0.04	4.30	6.28	6.32	0.04	6.30
4.32	4.36	0.04	4.34	6.32	6.36	0.04	6.34
4.36	4.40	0.04	4.38	6.36	6.40	0.04	6.38
4.40	4.44	0.04	4.42	6.40	6.44	0.04	6.42
4.44	4.48	0.04	4.46	6.44	6.48	0.04	6.46
4.48	4.52	0.04	4.50	6.48	6.52	0.04	6.50
4.52	4.56	0.04	4.54	6.52	6.56	0.04	6.54
4.56	4.60	0.04	4.58	6.56	6.60	0.04	6.58
4.60	4.64	0.04	4.62	6.60	6.64	0.04	6.62
4.64	4.68	0.04	4.66	6.64	6.68	0.04	6.66
4.68	4.72	0.04	4.70	6.68	6.72	0.04	6.70
4.72	4.76	0.04	4.74	6.72	6.76	0.04	6.74
4.76	4.80	0.04	4.78	6.76	6.80	0.04	6.78
4.80	4.84	0.04	4.82	6.80	6.84	0.04	6.82
4.84	4.88	0.04	4.86	6.84	6.88	0.04	6.86
4.88	4.92	0.04	4.90	6.88	6.92	0.04	6.90
4.92	4.96	0.04	4.94	6.92	6.96	0.04	6.94
4.96	5.00	0.04	4.98	6.96	7.00	0.08	6.98
5.00	5.04	0.04	5.02	7.00	7.08	0.08	7.04
5.04	5.08	0.04	5.06	7.08	7.16	0.08	7.12
5.08	5.12	0.04	5.10	7.16	7.24	0.08	7.20
5.12	5.16	0.04	5.14	7.24	7.32	0.08	7.28
5.16	5.20	0.04	5.18	7.32	7.40	0.08	7.36
5.20	5.24	0.04	5.22	7.40	7.48	0.08	7.44
5.24	5.28	0.04	5.26	7.48	7.56	0.08	7.52
5.28	5.32	0.04	5.30	7.56	7.64	0.08	7.60
5.32	5.36	0.04	5.34	7.64	7.72	0.08	7.68
5.36	5.40	0.04	5.38	7.72	7.80	0.08	7.76
5.40	5.44	0.04	5.42	7.80	7.88	0.08	7.84
5.44	5.48	0.04	5.46	7.88	7.96	0.08	7.92
5.48	5.52	0.04	5.50	7.96	8.04	0.08	8.00
5.52	5.56	0.04	5.54	8.04	8.12	0.08	8.08
5.56	5.60	0.04	5.58	8.12	8.20	0.08	8.16
5.60	5.64	0.04	5.62	8.20	8.28	0.08	8.24
5.64	5.68	0.04	5.66	8.28	8.36	0.08	8.32

Table A.2. Size Parameter (x) (continued)

Range		dx	x representing	Range		dx	x representing
lower	upper		range	lower	upper		range
8.36	8.44	0.08	8.40	11.56	11.64	0.08	11.60
8.44	8.52	0.08	8.48	11.64	11.72	0.08	11.68
8.52	8.60	0.08	8.56	11.72	11.80	0.08	11.76
8.60	8.68	0.08	8.64	11.80	12.00	0.20	11.90
8.68	8.76	0.08	8.72	12.00	12.20	0.20	12.10
8.76	8.84	0.08	8.80	12.20	12.40	0.20	12.30
8.84	8.92	0.08	8.88	12.40	12.60	0.20	12.50
8.92	9.00	0.08	8.96	12.60	12.80	0.20	12.70
9.00	9.08	0.08	9.04	12.80	13.00	0.20	12.90
9.08	9.16	0.08	9.12	13.00	13.20	0.20	13.10
9.16	9.24	0.08	9.20	13.20	13.40	0.20	13.30
9.24	9.32	0.08	9.28	13.40	13.60	0.20	13.50
9.32	9.40	0.08	9.36	13.60	13.80	0.20	13.70
9.40	9.48	0.08	9.44	13.80	14.00	0.20	13.90
9.48	9.56	0.08	9.52	14.00	14.20	0.20	14.10
9.56	9.64	0.08	9.60	14.20	14.40	0.20	14.30
9.64	9.72	0.08	9.68	14.40	14.60	0.20	14.50
9.72	9.80	0.08	9.76	14.60	14.80	0.20	14.70
9.80	9.88	0.08	9.84	14.80	15.00	0.20	14.90
9.88	9.96	0.08	9.92	15.00	15.20	0.20	15.10
9.96	10.04	0.08	10.00	15.20	15.40	0.20	15.30
10.04	10.12	0.08	10.08	15.40	15.60	0.20	15.50
10.12	10.20	0.08	10.16	15.60	15.80	0.20	15.70
10.20	10.28	0.08	10.24	15.80	16.00	0.20	15.90
10.28	10.36	0.08	10.32	16.00	16.20	0.20	16.10
10.36	10.44	0.08	10.40	16.20	16.40	0.20	16.30
10.44	10.52	0.08	10.48	16.40	16.60	0.20	16.50
10.52	10.60	0.08	10.56	16.60	16.80	0.20	16.70
10.60	10.68	0.08	10.64	16.80	17.00	0.20	16.90
10.68	10.76	0.08	10.72	17.00	17.40	0.40	17.20
10.76	10.84	0.08	10.80	17.40	17.80	0.40	17.60
10.84	10.92	0.08	10.88	17.80	18.20	0.40	18.00
10.92	11.00	0.08	10.96	18.20	18.60	0.40	18.40
11.00	11.08	0.08	11.04	18.60	19.00	0.40	18.80
11.08	11.16	0.08	11.12	19.00	19.40	0.40	19.20
11.16	11.24	0.08	11.20	19.40	19.80	0.40	19.60
11.24	11.32	0.08	11.28	19.80	20.20	0.40	20.00
11.32	11.40	0.08	11.36	20.20	20.60	0.40	20.40
11.40	11.48	0.08	11.44	20.60	21.00	0.40	20.80
11.48	11.56	0.08	11.52	21.00	21.40	0.40	21.20
				21.40	21.80	0.40	21.60
				21.80	22.40	0.40	22.00
				22.40	22.80	0.40	22.40

APPENDIX B : Water Table

Table B.1. Resolution and range of complex refractive index in the water table for frequencies lower and including 37 GHz

No.	Real refractive index Range		Increment for averaging	No.	Imaginary refractive index Range		Increment for averaging
	Lower	Upper			Lower	Upper	
1	2.0	2.4	0.1	1	1.2	1.5	0.1
2	2.4	2.7	0.1	2	1.4	1.7	0.1
				3	1.7	2.2	0.1
3	2.7	3.0	0.1	4	1.5	1.9	0.1
				5	1.9	2.4	0.1
4	3.0	3.3	0.1	6	1.7	2.1	0.1
5	3.3	3.6	0.1	7	2.0	2.3	0.1
				8	2.3	2.7	0.1
6	3.6	3.9	0.1	9	2.1	2.4	0.1
				10	2.4	2.9	0.1
7	3.9	4.2	0.1	11	2.3	2.7	0.1
				12	2.7	3.1	0.1
8	4.2	4.5	0.1	13	2.5	2.8	0.1
				14	2.8	3.2	0.1
9	4.5	4.8	0.1	15	2.6	3.0	0.1
				16	3.0	3.4	0.1
10	4.8	5.1	0.1	17	2.7	3.0	0.1
				18	3.0	3.4	0.1
11	5.1	5.4	0.1	19	2.7	3.0	0.1
				20	3.0	3.4	0.1
12	5.4	5.7	0.1	21	2.7	3.0	0.1
				22	3.0	3.5	0.1
13	5.7	6.0	0.1	23	2.7	3.0	0.1
				24	3.0	3.5	0.1
14	6.0	6.3	0.1	25	2.6	3.0	0.1
				26	3.0	3.5	0.1
15	6.3	6.6	0.1	27	2.6	3.0	0.1
				28	3.0	3.5	0.1
16	6.6	6.9	0.1	29	2.5	2.9	0.1
				30	2.9	3.4	0.1

Table B.1. (continued)

No.	Real refractive index			No.	Imaginary refractive index		
	Range		Increment for averaging		Range		Increment for averaging
	Lower	Upper			Lower	Upper	
17	6.9	7.2	0.1	31	2.3	2.7	0.1
				32	2.7	3.3	0.1
18	7.2	7.5	0.1	33	2.0	2.4	0.1
				34	2.4	2.8	0.1
				35	2.8	3.2	0.1
19	7.5	7.8	0.1	36	1.7	2.1	0.1
				37	2.1	2.6	0.1
				38	2.6	3.1	0.1
20	7.8	8.1	0.1	39	1.5	1.9	0.1
				40	1.9	2.4	0.1
				41	2.4	2.9	0.1
21	8.1	8.4	0.1	42	0.8	1.2	0.1
				43	1.2	1.7	0.1
				44	1.7	2.4	0.1
22	8.4	8.7	0.1	45	0.6	1.1	0.1
				46	1.1	1.6	0.1
				47	1.6	2.1	0.1

Table B.2. Same as Table B.1 except for size parameter

Range			Increment for	Range			Increment for
Lower	Upper	dx	averaging	Lower	Upper	dx	averaging
1.E-4	5.E-4	4.E-4	1.E-4	0.93	0.95	0.02	0.01
5.E-4	1.E-3	5.E-4	1.E-4	0.95	0.97	0.02	0.01
1.E-3	5.E-3	4.E-3	1.E-3	0.97	0.99	0.02	0.01
5.E-3	1.E-2	5.E-3	1.E-3	0.99	1.01	0.02	0.01
1.E-2	3.E-2	0.02	0.01	1.01	1.05	0.04	0.01
3.E-2	0.05	0.02	0.01	1.05	1.09	0.04	0.01
0.05	0.07	0.02	0.01	1.09	1.13	0.04	0.01
0.07	0.09	0.02	0.01	1.13	1.17	0.04	0.01
0.09	0.11	0.02	0.01	1.17	1.21	0.04	0.01
0.11	0.13	0.02	0.01	1.21	1.25	0.04	0.01
0.13	0.15	0.02	0.01	1.25	1.30	0.05	0.01
0.15	0.17	0.02	0.01	1.30	1.35	0.05	0.01
0.17	0.19	0.02	0.01	1.35	1.40	0.05	0.01
0.19	0.21	0.02	0.01	1.40	1.45	0.05	0.01
0.21	0.23	0.02	0.01	1.45	1.50	0.05	0.01
0.23	0.25	0.02	0.01	1.50	1.55	0.05	0.01
0.25	0.27	0.02	0.01	1.55	1.60	0.05	0.01
0.27	0.29	0.02	0.01	1.60	1.65	0.05	0.01
0.29	0.31	0.02	0.01	1.65	1.70	0.05	0.01
0.31	0.33	0.02	0.01	1.70	1.75	0.05	0.01
0.33	0.35	0.02	0.01	1.75	1.80	0.05	0.01
0.35	0.37	0.02	0.01	1.80	1.85	0.05	0.01
0.37	0.39	0.02	0.01	1.85	1.90	0.05	0.01
0.39	0.41	0.02	0.01	1.90	1.95	0.05	0.01
0.41	0.43	0.02	0.01	1.95	2.00	0.05	0.01
0.43	0.45	0.02	0.01	2.00	2.05	0.05	0.01
0.45	0.47	0.02	0.01	2.05	2.10	0.05	0.01
0.47	0.49	0.02	0.01	2.10	2.15	0.05	0.01
0.49	0.51	0.02	0.01	2.15	2.20	0.05	0.01
0.51	0.53	0.02	0.01	2.20	2.25	0.05	0.01
0.53	0.55	0.02	0.01	2.25	2.30	0.05	0.01
0.55	0.57	0.02	0.01	2.30	2.35	0.05	0.01
0.57	0.59	0.02	0.01	2.35	2.40	0.05	0.01
0.59	0.61	0.02	0.01	2.40	2.45	0.05	0.01
0.61	0.63	0.02	0.01	2.45	2.50	0.05	0.01
0.63	0.65	0.02	0.01	2.50	2.60	0.10	0.05
0.65	0.67	0.02	0.01	2.60	2.70	0.10	0.05
0.67	0.69	0.02	0.01	2.70	2.80	0.10	0.05
0.69	0.71	0.02	0.01	2.80	2.90	0.10	0.05
0.71	0.73	0.02	0.01	2.90	3.00	0.10	0.05
0.73	0.75	0.02	0.01	3.00	3.20	0.20	0.05
0.75	0.77	0.02	0.01	3.20	3.40	0.20	0.05
0.77	0.79	0.02	0.01	3.40	3.60	0.20	0.05
0.79	0.81	0.02	0.01	3.60	3.80	0.20	0.05
0.81	0.83	0.02	0.01	3.80	4.00	0.20	0.05
0.83	0.85	0.02	0.01	4.00	4.20	0.20	0.05
0.85	0.87	0.02	0.01	4.20	4.40	0.20	0.05
0.87	0.89	0.02	0.01	4.40	4.60	0.20	0.05
0.89	0.91	0.02	0.01	4.60	4.80	0.20	0.05
0.91	0.93	0.02	0.01	4.80	5.00	0.20	0.05

Table B.3. Same as Table B.1 except for frequency greater than 37 GHz

Real refractive index (n)			Imaginary refractive index (k)		
Range		Increment for	Range		Increment for
Lower	Upper	averaging	Lower	Upper	averaging
1.5	2.0	0.1	0.3	0.6	0.1
			0.6	0.9	0.1
			0.9	1.2	0.1
2.0	2.2	0.1	0.2	0.4	0.1
			0.4	0.6	0.1
			0.6	0.8	0.1
			0.8	1.0	0.1
			1.0	1.2	0.1
2.2	2.4	0.1	0.2	0.4	0.1
			0.4	0.6	0.1
			0.6	0.8	0.1
			0.8	1.0	0.1
			1.0	1.2	0.1
			1.2	1.4	0.1
2.4	2.6	0.1	0.8	1.0	0.1
			1.0	1.2	0.1
			1.2	1.4	0.1
			1.4	1.6	0.1
2.6	2.8	0.1	0.8	1.0	0.1
			1.0	1.2	0.1
			1.2	1.4	0.1
			1.4	1.6	0.1
			1.6	1.8	0.1
2.8	3.0	0.1	1.3	1.5	0.1
			1.5	1.7	0.1
			1.7	1.9	0.1
3.0	3.5	0.1	1.6	1.8	0.1
			1.8	2.0	0.1
			2.0	2.2	0.1
3.5	4.0	0.1	2.0	2.5	0.1
4.0	4.5	0.1	2.3	2.7	0.1
4.5	5.0	0.1	2.5	2.8	0.1
5.0	5.5	0.1	2.7	2.9	0.1
5.5	6.2	0.1	2.7	2.9	0.1

Table B.4. Same as Table B.2 except for the frequencies higher than 37 GHz

Range			Increment for	Range			Increment for
Lower	Upper	Averaging	averaging	Lower	Upper	Averaging	averaging
1.E-4	5.E-4	5.E-4	1.E-4	2.60	2.70	0.10	0.05
5.E-4	1.E-3	5.E-4	1.E-4	2.70	2.80	0.10	0.05
1.E-3	5.E-3	5.E-3	1.E-3	2.80	2.90	0.10	0.05
5.E-3	1.E-2	5.E-3	1.E-3	2.90	3.00	0.10	0.05
1.E-2	5.E-2	5.E-2	1.E-3	3.00	3.20	0.20	0.05
5.E-2	1.E-1	5.E-2	1.E-3	3.20	3.40	0.20	0.05
0.10	0.15	0.05	0.01	3.40	3.60	0.20	0.05
0.15	0.20	0.05	0.01	3.60	3.80	0.20	0.05
0.20	0.25	0.05	0.01	3.80	4.00	0.20	0.05
0.25	0.30	0.05	0.01	4.00	4.20	0.20	0.05
0.30	0.35	0.05	0.01	4.20	4.40	0.20	0.05
0.35	0.40	0.05	0.01	4.40	4.60	0.20	0.05
0.40	0.45	0.05	0.01	4.60	4.80	0.20	0.05
0.45	0.50	0.05	0.01	4.80	5.00	0.20	0.05
0.50	0.55	0.05	0.01	5.00	5.30	0.30	0.1
0.55	0.60	0.05	0.01	5.30	5.60	0.30	0.1
0.60	0.65	0.05	0.01	5.60	5.90	0.30	0.1
0.65	0.70	0.05	0.01	5.90	6.20	0.30	0.1
0.70	0.75	0.05	0.01	6.20	6.50	0.30	0.1
0.75	0.80	0.05	0.01	6.50	7.00	0.50	0.1
0.80	0.85	0.05	0.01	7.00	7.50	0.50	0.1
0.85	0.90	0.05	0.01	7.50	8.00	0.50	0.1
0.90	0.95	0.05	0.01	8.00	8.50	0.50	0.1
0.95	1.00	0.05	0.01	8.50	9.00	0.50	0.1
1.00	1.10	0.05	0.05	9.00	10.0	1.0	0.20
1.10	1.20	0.05	0.05	10.0	11.0	1.0	0.20
1.20	1.30	0.05	0.05	11.0	12.0	1.0	0.20
1.30	1.40	0.05	0.05	12.0	14.0	2.0	0.20
1.40	1.50	0.05	0.05	14.0	16.0	2.0	0.20
1.50	1.60	0.10	0.05	16.0	18.0	2.0	0.20
1.60	1.70	0.10	0.05	18.0	20.0	2.0	0.20
1.70	1.80	0.10	0.05				
1.80	1.90	0.10	0.05				
1.90	2.00	0.10	0.05				
2.00	2.10	0.10	0.05				
2.10	2.20	0.10	0.05				
2.20	2.30	0.10	0.05				
2.30	2.40	0.10	0.05				
2.40	2.50	0.10	0.05				
2.50	2.60	0.10	0.05				

APPENDIX C

Table C.1 VARIABLE ORGANIZATION

RFR : Real refractive index
RFI : Imaginary refractive index
X : Size parameter
QEXT : Extinction efficiency factor
QSCAT : Scattering efficiency factor
PHAFN : 4 elements of phase function

Note : All variables are averaged variables. Each set of variables constitute a record.

RFR$_1$, RFI$_1$, X$_1$, QEXT$_{111}$, QSCAT$_{111}$, PHAFN$_{111}$,
X$_2$, QEXT$_{112}$, QSCAT$_{112}$, PHAFN$_{112}$,
X$_3$, QEXT$_{113}$, QSCAT$_{113}$, PHAFN$_{113}$,
.
.
.
X$_S$, QEXT$_{11S}$, QSCAT$_{11S}$, PHAFN$_{11S}$,
RFI$_2$, X$_1$, QEXT$_{121}$, QSCAT$_{121}$, PHAFN$_{121}$,
X$_2$, QEXT$_{122}$, QSCAT$_{122}$, PHAFN$_{122}$,
X$_3$, QEXT$_{123}$, QSCAT$_{123}$, PHAFN$_{123}$,
.
.
.
X$_S$, QEXT$_{12S}$, QSCAT$_{12S}$, PHAFN$_{12S}$,
.
.
.
RFI$_D$, X$_1$, QEXT$_{1D1}$, QSCAT$_{1D1}$, PHAFN$_{1D1}$,
X$_2$, QEXT$_{1D2}$, QSCAT$_{1D2}$, PHAFN$_{1D2}$,
X$_3$, QEXT$_{1D3}$, QSCAT$_{1D3}$, PHAFN$_{1D3}$,
.
.
.
X$_S$, QEXT$_{1DS}$, QSCAT$_{1DS}$, PHAFN$_{1DS}$,

RFR$_2$, RFI$_1$, X$_1$, QEXT$_{211}$, QSCAT$_{211}$, PHAFN$_{211}$,
X$_2$, QEXT$_{212}$, QSCAT$_{212}$, PHAFN$_{212}$,
X$_3$, QEXT$_{213}$, QSCAT$_{213}$, PHAFN$_{213}$,
.
.
.
X$_S$, QEXT$_{21S}$, QSCAT$_{21S}$, PHAFN$_{21S}$,

Table C.1 (continued)

```
      RFI , X , QEXT    , QSCAT    , PHAFN    ,
         2  1      221        221        221
            X , QEXT    , QSCAT    , PHAFN    ,
             2      222        222        222
            X , QEXT    , QSCAT    , PHAFN    ,
             3      223        223        223
            .
            .
            .
            X , QEXT    , QSCAT    , PHAFN    ,
             S      22S        22S        22S
      .
      .
      .
      RFI , X , QEXT    , QSCAT    , PHAFN    ,
         E  1      2E1        2E1        2E1
            X , QEXT    , QSCAT    , PHAFN    ,
             2      2E2        2E2        2E2
            X , QEXT    , QSCAT    , PHAFN    ,
             3      2E3        2E3        2E3
            .
            .
            .
            X , QEXT    , QSCAT    , PHAFN    ,
             S      2ES        2ES        2ES
RFR , RFI , X , QEXT    , QSCAT    , PHAFN    ,
   3    1  1      311        311        311
            X , QEXT    , QSCAT    , PHAFN    ,
             2      312        312        312
            X , QEXT    , QSCAT    , PHAFN    ,
             3      313        313        313
            .
            .
            .
            X , QEXT    , QSCAT    , PHAFN    ,
             S      31S        31S        31S
      RFI , X , QEXT    , QSCAT    , PHAFN    ,
         2  1      321        321        321
            X , QEXT    , QSCAT    , PHAFN    ,
             2      322        322        322
            X , QEXT    , QSCAT    , PHAFN    ,
             3      323        323        323
            .
            .
            .
            X , QEXT    , QSCAT    , PHAFN    ,
             S      32S        32S        32S
      .
      .
      .
      RFI , X , QEXT    , QSCAT    , PHAFN    ,
         P  1      3P1        3P1        3P1
            X , QEXT    , QSCAT    , PHAFN    ,
             2      3P2        3P2        3P2
            X , QEXT    , QSCAT    , PHAFN    ,
             3      3P3        3P3        3P3
            .
            .
            .
            X , QEXT    , QSCAT    , PHAFN    ,
             S      3PS        3PS        3PS
```

Table C.1 (continued)

```
.
.
.
RFR , RFI , X , QEXT    , QSCAT    , PHAFN    ,
   I     1   1       I11        I11        I11
             X , QEXT    , QSCAT    , PHAFN    ,
              2       I12        I12        I12
             X , QEXT    , QSCAT    , PHAFN    ,
              3       I13        I13        I13
             .
             .
             .
             X , QEXT    , QSCAT    , PHAFN    ,
              S       I1S        I1S        I1S
       RFI , X , QEXT    , QSCAT    , PHAFN    ,
          2   1       I21        I21        I21
             X , QEXT    , QSCAT    , PHAFN    ,
              2       I22        I22        I22
             X , QEXT    , QSCAT    , PHAFN    ,
              3       I23        I23        I23
             .
             .
             .
             X , QEXT    , QSCAT    , PHAFN    ,
              S       I2S        I2S        I2S
       .
       .
       .
       RFI , X , QEXT    , QSCAT    , PHAFN    ,
          Z   1       IZ1        IZ1        IZ1
             X , QEXT    , QSCAT    , PHAFN    ,
              2       IZ2        IZ2        IZ2
             X , QEXT    , QSCAT    , PHAFN    ,
              3       IZ3        IZ3        IZ3
             .
             .
             .
             X , QEXT    , QSCAT    , PHAFN    ,
              S       IZS        IZS        IZS
```

Table C.2 Mie table specifications

ICE

Data set name	:	MIET.ICE
Organization	:	Direct access
Logical record length*	:	1460
Blocksize	:	20440
Number of records per block	:	14
Number of records	:	2681
Number of blocks	:	200
Record format	:	Fixed Block (FB)

WATER (less than and including 37 GHz)

Data set name	:	MIETWL37
Organization	:	Direct access
Logical record length*	:	340
Blocksize	:	23120
Number of records per block	:	68
Number of records	:	4700
Number of blocks	:	70
Record format	:	Fixed Block (FB)

WATER (greater than 37 GHz)

Data set name	:	MIETWG37
Organization	:	Direct Access
Logical record length*	:	1460
Blocksize	:	20440
Number of records per block	:	14
Number of records	:	2414
Number of blocks	:	180
Record format	:	Fixed block (FB)

* A Word is 4 bytes (single precision). Each record contains variables in the following order.

Word	Variable
1	Real refractive index
2	Imaginary refractive index
3	Size parameter
4	Extinction efficiency factor
5	Scattering efficiency factor
6-IWORD	4 phase functions (IANG Scattering angles)

IWORD : IANG*4 + 5
IANG : 90 for ice
: 20 for water ; Frequency less than and including 37 GHz
: 90 for water : Frequency > 37 GHZ

Table C.3

NASA SPACE AND EARTH SCIENCES COMPUTING CENTER

COMPUTING UNIT ACCRUAL TABLE

FY87

RESOURCE	CYBER 205	IBM 3081	AMDAHL V6/V7
CPU (BATCH)	3.0 CU/CPU-HOUR	1.0 CU/CPU-HOUR	0.5 CU/CPU-HOUR
CPU (TSO)	N/A	1.2 CU/CPU-HOUR	0.6 CU/CPU-HOUR
TAPE	N/A	1.0 CU/500K EXCP	0.5 CU/500K EXCP
DISK (BATCH)	N/A	1.0 CU/250K EXCP	0.5 CU/250K EXCP
DISK (TSO)	N/A	1.0 CU/500K EXCP	0.5 CU/500K EXCP
OTHER	N/A	1.0 CU/500K EXCP	0.5 CU/500K EXCP
CONNECT TIME	N/A	1.0 CU/1000 HR	0.5 CU/1000 HR
TAPE MOUNT	N/A	1.0 CU/500 MOUNTS	1.0 CU/500 MOUNT
MEMORY	N/A	1.0 CU/50M BYTES/HR	0.5 CU/50M BYTES/HR
PAPER	N/A	1.0 CU/50K PAGES	1.0 CU/50K PAGES
TPUT/TGET	N/A	0.5 CU/500K EXCP	0.25 CU/500K EXCP
MINIMUM CHARGE	N/A	1.0 CU/1250 JOBS	0.5 CU/1250 JOBS

CLASS/PRIORITY CHARGES

NL	3.0 *	NORMAL RATE, CYBER 205 ONLY, FULL MACHINE JOBS
N	2.0 *	NORMAL RATE
E	0.5 *	NORMAL RATE *
F	0.2 *	NORMAL RATE *

ALL OTHER CLASSES ACCUMULATE CHARGE AT THE NORMAL RATE

* CLASS E & F RATES CHANGED AS OF APRIL 1, 1987

NASA National Aeronautics and Space Administration

Report Documentation Page

1. Report No.	2. Government Accession No.	3. Recipient's Catalog No.
NASA CR-4130		

4. Title and Subtitle

TABULATION OF MIE SCATTERING CALCULATION RESULTS FOR MICROWAVE RADIATIVE TRANSFER MODELING

5. Report Date

March 1988

6. Performing Organization Code

7. Author(s)

Hwa-Young M. Yeh and N. Prasad

8. Performing Organization Report No.

88B0116

10. Work Unit No.

9. Performing Organization Name and Address

Caelum Research Corporation, Silver Spring, MD, 20906
and
General Sciences Corporation, Laurel, MD, 20707

11. Contract or Grant No.

NAS5-30143
NAS5-28795

13. Type of Report and Period Covered

Contractor Report

12. Sponsoring Agency Name and Address

National Aeronautics and Space Administration
Washington, D.C. 20546-0001

14. Sponsoring Agency Code

15. Supplementary Notes

Hwa-Young M. Yeh is affiliated with Caelum Research Corporation, Silver Spring, Maryland, 20906.
N. Prasad is affiliated with General Sciences Corporation, Laurel, Maryland, 20707.

16. Abstract In microwave radiative transfer model simulations, the Mie calculations usually consume the majority of the computer time necessary for the calculations (70 to 86% for frequencies ranging from 6.6 to 183 GHz). For a large array of atmospheric profiles, the repeated calculations of the Mie codes make the radiative transfer computations not only expensive, but sometimes impossible. It is desirable, therefore, to develop a set of Mie tables to replace the Mie codes for the designated ranges of temperature and frequency in the microwave radiative transfer calculation. Results of using the Mie tables in the transfer calculations show that the total CPU time (IBM 3081) used for the modeling simulation is reduced by a factor of 7 to 16, depending on the frequency. The tables are tested by computing the upwelling radiance of 144 atmospheric profiles generated by a three-dimensional cloud model (Tao, 1986). Results are compared with those using Mie quantities computed from the Mie codes. The bias and root-mean-square deviation (RMSD) of the model results using the Mie tables, in general, are less than 1 K except for 37 and 90 GHz. Overall, neither the bias nor RMSD is worse than 1.7 K for any frequency and any viewing angle.

17. Key Words (Suggested by Author(s))

Mie calculations, microwave radiative transfer model, Mie table, size parameters, refractive index

18. Distribution Statement

Unclassified - Unlimited

Subject Category 47

19. Security Classif. (of this report)	20. Security Classif. (of this page)	21. No. of pages	22. Price
Unclassified	Unclassified	98	A05

NASA FORM 1626 OCT 86

NASA-Langley, 1988